Journal of Visualized Experiments

Patient-Specific Modeling of the Heart: Estimation of Ventricular Fiber Orientations

--Manuscript Draft--

Manuscript Number:	JoVE50125R1
Full Title:	Patient-Specific Modeling of the Heart: Estimation of Ventricular Fiber Orientations
Article Type:	Methods Article - JoVE Produced Video
Corresponding Author:	Fijoy Vadakkumpadan, PhD Johns Hopkins University Baltimore, MD UNITED STATES
Corresponding Author Secondary Information:	
Corresponding Author's Institution:	Johns Hopkins University
Corresponding Author's Secondary Institution:	
First Author:	Fijoy Vadakkumpadan, PhD
First Author Secondary Information:	
Order of Authors Secondary Information:	
Abstract:	Patient-specific simulations of heart (dys)function aimed at personalizing cardiac therapy are hampered by the absence of in vivo imaging technology for clinically acquiring myocardial fiber orientations. The objective of this project was to develop a methodology to estimate cardiac fiber orientations from in vivo images of patient heart geometries. An accurate representation of ventricular geometry and fiber orientations was reconstructed, respectively, from high-resolution ex vivo structural magnetic resonance (MR) and diffusion tensor (DT) MR images of a normal human heart, referred to as the atlas. Ventricular geometry of a patient heart was extracted, via semiautomatic segmentation, from an in vivo computed tomography (CT) image. Using image transformation algorithms, the atlas ventricular geometry was deformed to match that of the patient. Finally, the deformation field was applied to the atlas fiber orientations to obtain an estimate of patient fiber orientations. The accuracy of the fiber estimates was assessed using six normal and three failing canine hearts. The mean absolute difference between inclination angles of acquired and estimated fiber orientations was 15.4°. Computational simulations of ventricular activation maps and pseudo-ECGs in sinus rhythm and ventricular tachycardia indicated that there are no significant differences between estimated and acquired fiber orientations at a clinically observable level. The new insights obtained from the project will pave the way for the development of patient-specific models of the heart that can aid physicians in personalized diagnosis and decisions regarding electrophysiological interventions.
Corresponding Author E-Mail:	tofijoy@gmail.com
Other Authors:	Hermenegild Arevalo, MS
	Natalia Trayanova, PhD

Dear Meghan,

Please find enclosed the revision of our manuscript titled “Patient-Specific Modeling of the Heart: Estimation of Ventricular Fiber Orientations,” following our correspondence via e-mail. Also included is a point-by-point response to the comments from the reviewers. We look forward to hearing from you. Thank you.

Sincerely,

Fijoy Vadakkumpadan, PhD

Patient-Specific Modeling of the Heart: Estimation of Ventricular Fiber Orientations

Authors:

Fijoy Vadakkumpadan, Hermenegild Arevalo, Natalia Trayanova

Authors: institution(s)/affiliation(s) for each author:

Fijoy Vadakkumpadan
Institute for Computational Medicine and the Department of Biomedical Engineering
Johns Hopkins University, Baltimore, Maryland, USA
fijoy@jhu.edu

Hermenegild Arevalo
Institute for Computational Medicine and the Department of Biomedical Engineering
Johns Hopkins University, Baltimore, Maryland, USA
hermenegild@jhu.edu

Natalia Trayanova
Institute for Computational Medicine and the Department of Biomedical Engineering
Johns Hopkins University, Baltimore, Maryland, USA
ntrayanova@jhu.edu

Corresponding author:

Fijoy Vadakkumpadan

Keywords:

Cardiomyocyte, magnetic resonance imaging, biomedical image processing, patient-specific modeling, electrophysiology, simulation

Short Abstract:

A methodology to estimate ventricular fiber orientations from in vivo images of patient heart geometries for personalized modeling is described. Validation of the methodology performed using normal and failing canine hearts demonstrate that that there are no significant differences between estimated and acquired fiber orientations at a clinically observable level.

Long Abstract:

Patient-specific simulations of heart (dys)function aimed at personalizing cardiac therapy are hampered by the absence of in vivo imaging technology for clinically acquiring myocardial fiber orientations. The objective of this project was to develop a methodology to estimate cardiac fiber orientations from in vivo images of patient heart geometries. An accurate representation of ventricular geometry and fiber orientations was reconstructed, respectively, from high-resolution ex vivo structural magnetic resonance (MR) and diffusion tensor (DT) MR images of a normal human heart, referred to as the atlas. Ventricular geometry of a patient heart was extracted, via semiautomatic segmentation, from an in vivo computed tomography (CT) image. Using image transformation algorithms, the atlas ventricular geometry was deformed to match that of the patient. Finally, the deformation field was applied to the atlas fiber orientations to obtain an estimate of patient fiber orientations. The accuracy of the fiber estimates was assessed using six normal and three failing canine hearts. The mean absolute difference between inclination angles of acquired and estimated fiber orientations was 15.4°. Computational simulations of ventricular activation maps and pseudo-ECGs in sinus rhythm and ventricular tachycardia indicated that there are no significant differences between estimated and acquired fiber orientations at a clinically observable level. The new insights obtained from the project will pave the way for the development of patient-specific models of the heart that can aid physicians in personalized diagnosis and decisions regarding electrophysiological interventions.

Introduction:

The computational approach is becoming central to the advancement of the understanding of the function of the heart in health and disease. State-of-the-art whole-heart models of electrophysiology and electromechanics are currently being used to study a wide range of phenomena, such as normal ventricular propagation, arrhythmia, defibrillation, electromechanical coupling, and cardiac resynchronization [1]. However, for the computational approach to be directly applicable in the clinical environment, it is imperative that the models be patient-specific, i.e. the models must be based on the specific architecture and electrophysiological or electromechanical properties of the patient's diseased heart. Simulation with such models will aid physicians to arrive at highly personalized decisions for electrophysiological interventions as well as prophylaxis, thereby dramatically improving cardiac health care [2-4].

Creation of realistic cardiac models requires the acquisition of the geometry and fiber structure of a patient heart. Fiber orientations determine directions of electrical propagation and strain distributions in the heart, and therefore acquiring them is essential to cardiac modeling [5, 6]. With recent advances in medical imaging, it is now feasible to obtain the geometry of a patient

heart, including structural remodeling such as infarction, in vivo with high resolution using magnetic resonance imaging (MRI) and computed tomography (CT) technologies. However, there is no practical method for acquiring fiber structure of a patient heart in vivo. Diffusion tensor (DT) MRI [7, 8], the only technique to acquire fiber orientations of the intact heart, is not widely available in vivo due to certain limitations [9]. A brief description of the previous efforts to translate DTMRI to the clinical setting can be found elsewhere [2]. Though methodologies such as rule-based assignment of fiber orientations offer alternatives to DTMRI, these methodologies have certain serious limitations [2, 10]. Thus difficulties in acquiring cardiac fiber structure in vivo presently impede the application of electrophysiological and electromechanical cardiac simulations in clinical setting. The objective of this research was to directly address this need.

We hypothesized that ventricular fiber orientations of a heart can be accurately predicted given the geometry of the heart and an atlas, where the atlas is a heart whose geometry and fiber orientations are available. Accordingly, we used state of the art techniques to develop a methodology for estimation of cardiac fiber orientations in vivo, and tested the hypothesis in normal and failing canine ventricles [2]. The central idea of our fiber estimation methodology is to exploit similarities in fiber orientations, relative to geometry, between different hearts in order to approximate the fiber structure of a (target) heart for which only the geometry information is available. At the heart of our estimation methodology is the registration of the atlas geometry with the target geometry using large deformation diffeomorphic metric mapping (LDDMM) [11], and the morphing of atlas fiber orientations using preservation of principal components (PPD) [2, 12]. The diffeomorphic property of LDDMM guarantees that the atlas does not “fold over” itself during deformation, thereby preserving the integrity of anatomical structures. Fig. 1 illustrates the processing pipeline of our methodology. The protocol text section §1 describes the various components of the pipeline by demonstrating how the estimation can be performed for an example patient. The numbers inside some of the blocks in Fig. 1 refer to the corresponding subsections under section §1 of the protocol text.

We evaluated the performance of the proposed methodology by quantifying the estimation error, and measuring the effect of this error on simulations of cardiac electrophysiology, by computationally simulating local electrical activation maps as well as pseudo-electrocardiograms (pseudo-ECGs). Due to the unavailability of human hearts, the performance evaluation was conducted using canine hearts available from previous studies [13-15]. The estimation error was calculated by means of inclination angles [16], following the tradition of histology, where angular measurements are performed on tissue sections that are cut parallel to the epicardial surface. Since the angle between the fiber direction and epicardial tangent plane is generally small [17, 18], the information loss in describing a fiber direction entirely using its inclination angle is insignificant. For the computational simulations, image-based

models were built as reported previously [19, 20], and cardiac tissue in the models was represented based on established mathematical techniques and experimental data [21-25]. Sinus rhythm was simulated by replicating activation originating from the Purkinje network [26], and ventricular tachycardia, by an S1-S2 pacing protocol [27]. Pseudo-ECGs were computed [28] and compared using the mean absolute deviation (MAD) metric [29].

Protocol Text:

1.) Fiber Orientations Estimation

1.1) Acquire structural MRI and DTMRI images of a normal adult human heart in diastole, at a resolution of $1mm^3$. Using ImageJ, extract the ventricular myocardium from the atlas structural image by fitting, for each short-axis slice, closed splines through a set of landmark points placed along the epicardial and endocardial boundaries in the slice (Fig. 2A & Fig. 2B). Perform the placement of landmark points manually for every 10^{th} slice in the image. Obtain the landmark points for the remaining slices by linearly interpolating the manually identified points, using MATLAB®. Reconstruct the fiber orientations of the atlas heart by computing the primary eigenvectors of the DTs in the DTMRI image (Fig. 2C).

1.2) Acquire an image of the geometry of the patient heart in diastole using in vivo cardiac CT or MRI. Reconstruct the patient heart geometry from the image similarly to the way the atlas was built (Fig. 3A & Fig. 3B). The patient image should be re-sampled prior to reconstruction such that the in-plane resolution is $1mm^2$. Similarly, the number of slices for which landmarks are manually picked, and the interval of out-of-plane interpolation must be adjusted so that the segmented patient heart image has a slice thickness of 1mm.

1.3) Deform the atlas ventricular image to match the patient geometry image in two steps. In the first step, perform an affine transformation based on a set of thirteen landmarks points: the left ventricular (LV) apex, the two right ventricular (RV) insertion points at the base, the two RV insertion points midway between base and apex, and four sets of two points that evenly divide RV and LV epicardial contours at base, and midway between base and apex (Fig. 4A & Fig. 4B). In the second step, deform the affine-transformed atlas ventricles further to match the patient geometry, using large deformation diffeomorphic metric mapping (LDDMM) (Fig. 4C).

1.4) Morph the DTMRI image of the atlas by re-positioning of image voxels and re-orientating the DTs according to the transformation matrix of the affine matching and the deformation field of the LDDMM transformation. Perform the re-orientation of the DTs using the preservation of principal directions (PPD) method.

1.5) Obtain the estimate of the patient fiber orientations from the morphed atlas DTMRI image by computing the primary eigenvector of the DTs (Fig. 5).

2.) Measurement of Estimation Error

2.1.) Acquire ex vivo structural MR and DTMR images of six normal and three failing canine hearts, at a resolution of 312.5×312.5×800μm^3. Here, heart failure should be generated in the canines via radiofrequency ablation of the left bundle-branch followed by 3 weeks of tachypacing at 210 minutes^{-1}.

2.2.) Segment the ventricles from the canine hearts similarly to the human atlas heart, as described in §1.1. Denote ventricles segmented from normal canine hearts as hearts 1 through 6, and those segmented from failing canine hearts as hearts 7 through 9 (Fig. 6).

2.3.) Obtain five different estimates of ventricular fiber orientations of heart 1 by using each of hearts 2 to 6 as an atlas (Fig. 7).

2.4.) Estimate fiber orientations for each of the failing ventricles using heart 1 as the atlas (Fig. 8).

2.5.) For each data point in each set of estimated fiber orientations, compute the estimation error as $|\theta_e - \theta_a|$, where $\theta_e$and θ_a are the inclination angles of estimated and acquired fiber orientations at that point, respectively.

2.6) For each data point in each set of estimated fiber orientations, compute the acute angle between estimated and acquired fiber directions in three-dimensions (3D) by means of the vector dot product.

3.) Measurement of the Effects of Estimation Error on Simulations

3.1.) From heart 1, construct six models, one with the DTMRI-acquired fiber orientations of heart 1 (referred to as model 1), and five with the five estimated fiber orientations datasets (models 2 to 6). For each of the three failing heart geometries, construct two ventricular models, one with the DTMRI-acquired fiber orientations and the other with the estimated fiber orientations. Here the spatial resolution of the models, computed in terms of the average edge length of the meshes, should be about 600μm. Denote the heart failure models with DTMRI-acquired fibers as models 7 to 9, and those with estimated fibers as models 10 to 12. In the models, use monodomain representation to describe the cardiac tissue, with governing equations:

$$C_m \frac{\delta V_m}{\delta t} + I_{ion} = \nabla \cdot (\sigma_b \nabla V_m)$$

$$I_{ion} = I_{ion}(V_m, \mu)$$

$$\frac{\delta \mu}{\delta t} = G(V_m, \mu)$$

where σ_b is the bulk conductivity tensor which is calculated from the bidomain conductivity tensors as described by Potse et al [30]; V_m is the transmembrane potential; C_m is the membrane specific capacitance; and I_{ion} is the density of the transmembrane current, which in turn depends on V_m and a set of state variables μ describing the dynamics of ionic fluxes across the membrane. For C_m, use a value of 1 μF/cm^2. For σ_i in normal canine heart models, use longitudinal and transverse conductivity values of 0.34 S/m and 0.06 S/m, respectively. Represent I_{ion} by the Greenstein-Winslow ionic models of the canine ventricular myocyte. Decrease the electrical conductivities in canine heart failure ventricular models by 30%. (Fig. 9)

3.2.) Using the software package CARP (CardioSolv, LLC), simulate sinus rhythm with all models. Induce reentrant ventricular tachycardia (VT) in the six failing models using an S1-S2 pacing protocol. Choose the timing between S1 and S2 to obtain sustained VT activity for 2 seconds after S2 delivery. If VT is not induced for any S1-S2 timing, decrease the conductivities by up to 70% until VT was induced (Fig. 10).

3.3.) For each simulation, calculate pseudo-ECGs by taking the difference of extracellular potentials between two points in an isotropic bath surrounding the hearts. Place the two points near the base of the heart separated by 18cm, such that the line connecting them is perpendicular to the base-apex plane of the septum as illustrated in Fig. 10. For each simulation with estimated fiber orientations, compute the MAD metric as

$$\text{MAD} = \frac{\sum_{i=1}^{n} |(X_i - \bar{X}) - (Y_i - \bar{Y})|}{\sum_{i=1}^{n} (|X_i - \bar{X}| + |Y_i - \bar{Y}|)}$$

where *X* is the ECG waveform of the simulation with estimated fiber orientations, *Y* is the ECG waveform of the corresponding simulation with acquired fiber orientations, $\bar{X}$ is the mean value of *X*, $\bar{Y}$ is the mean value of *Y*, and *n* is the length of *X* and *Y*.

Representative Results:

Fig. 11, A-C displays streamlined visualizations of estimated as well as DTMRI-derived fiber orientations in normal and failing hearts. Qualitative examination shows that estimated fiber orientations align well with DTMRI-derived ones. Panel D illustrates, overlaid on the geometry of heart 1, the distribution of error in normal hearts' inclination angles, averaged across all five estimates. Panel E shows the mean distribution of error in failing hearts' inclination angles, overlaid on the geometry of heart 1. Note that inclination angles have values between -90^o and +90^o, and therefore, the estimation error ranges between 0^o and 180^o. Panels F and G present sections of tissue from the distributions in panels D and E, respectively. This highlights the transmural variation of error. The histograms of errors in panel H suggest that most myocardial voxels have small error values. About 80% and 75% of the voxels have errors less than 20° in normal and failing ventricles, respectively. It was found that the mean error, averaged across all

estimated datasets, and all image voxels that belonged to the myocardium, were 14.4° and 16.9° in normal and failing ventricles, respectively. The mean error in the entire myocardium, in normal and failing cases combined, was 15.4°. The mean 3D acute angle between estimated and acquired fiber directions were 17.5^{o} and 18.8^{o} in normal and failing ventricles, respectively. The 3-D angles are comparable to the estimation errors. These results show that inclination angles of predicted fiber orientations are comparable to those acquired by ex-vivo DTMRI, the state-of-the-art technique. The standard deviation of error across the five different estimates of the fiber orientations of heart 1 was only 1.9 indicating that the variation in estimation quality from one atlas to another is small.

Figs. 12 and 13 present the simulated activation maps of one beat of sinus rhythm activation in normal and failing ventricular models, respectively. Models with estimated fiber orientations produce activation maps very similar to those of models with acquired orientations; the earliest epicardial activations occur at the same sites, and the directions of propagation match as well. The overall mean difference in total activation times between the acquired and estimated fiber orientation cases in the normal ventricular models, averaged over all estimates and all mesh nodes, was 5.7ms, which is a small fraction (3.7% on average) of the total activation time. Fig. 12C demonstrates that pseudo-ECGs obtained for sinus rhythm simulations with models 1 and 3 have identical morphologies. The MAD score between these two waveforms was 4.14%. On average, the MAD score between sinus rhythm pseudo-ECGs with each of models 2 to 6 and model 1 was 10.9%. In simulations of sinus rhythm with failing ventricular models, the mean difference in total activation times between models with acquired and estimated fiber orientations was only 5.2ms (3.1%), while the mean MAD score was 4.68%. These results indicate that the outcomes of simulation of ventricular activation in sinus rhythm in normal and failing canine ventricular models with fiber orientations estimated with the present methodology closely match those with acquired orientations. In particular, presence of heart failure did not diminish the accuracy of the estimation.

Fig. 14 shows simulated activation maps, in apical views of the ventricles, during one cycle of induced VT in the heart failure models, and corresponding pseudo-ECGs. Simulations with acquired and estimated fiber orientation both exhibit similar figure-of-eight reentrant patterns. The ECG morphologies corresponding to estimated and acquired fiber orientations were in good agreement. The mean MAD score was 9.3%. These results indicate that canine heart failure models with estimated fiber orientations can closely replicate outcomes of VT simulations performed using acquired fiber orientations.

Tables and Figures:

Figure 1: Our processing pipeline for estimating ventricular fiber orientations in vivo.

Figure 2: Geometry and fiber orientations of the atlas ventricles. (A) The epicardial (red) and endocardial (green and magenta) splines, and corresponding landmarks (yellow) overlaid on an example slice of the atlas image. (B) The atlas ventricles in 3D. (C) The atlas fiber orientations.

Figure 3: Patient ventricular geometry reconstruction. (A) The epicardial (red) and endocardial (green and magenta) splines, and corresponding landmarks (yellow) overlaid on an image slice. (B) Patient ventricles in 3D.

Figure 4: Deformation of the atlas ventricles to match the patient ventricles. (A) Superimposition of ventricles of atlas (magenta, see Fig. 2B) and patient (red, see Fig. 3B). (B) Patient ventricles and the affine transformed atlas ventricles. (C) Patient ventricles and LDDMM-transformed atlas ventricles.

Figure 5: Estimated fiber orientations of the patient heart in Fig. 3B.

Figure 6: Segmentation of canine hearts. The epicardial (blue) and endocardial (red and magenta) splines, and corresponding landmarks (green) overlaid on an example slice of a normal canine heart.

Figure 7: The acquired and estimated fiber orientations of heart 1.

Figure 8: The acquired and estimated fiber orientations of hearts 7-9.

Figure 9: Left panel illustrates the computational mesh generated for the models of heart 1. On the right, the action potential curve of normal canine ventricular myocardium computed using the Greenstein-Winslow model is displayed.

Figure 10: Pacing sites of the simulation of sinus rhythm and VT, as overlaid on the geometry of heart 7. E1E2 illustrates the lead vector used in pseudo-ECG calculations

Figure 11: Validation of the fiber orientation estimation methodology by comparing estimated fiber orientations with DTMRI-derived orientations. (A) Superimposition of DTMRI-acquired fiber orientations (greenish yellow) and one set of estimated fiber orientations (cyan) of heart 1. (B) Acquired and estimated fiber orientations of heart 7. (C) An enlarged portion of (B) showing alignment between acquired and estimated fiber orientations. Note that the streamlines were generated at random locations within the myocardium for visualization purposes only, and so their exact positions are irrelevant. (D) Distribution of mean estimation error in normal ventricles. (E) Distribution of mean estimation error in failing ventricles. (F) A section of tissue extracted from (D). (G) A section of tissue extracted from (E). The colorbar applies to D-G. (H) Histograms of errors in normal and failing ventricles. Frequency denotes the number of voxels having a given error.

Figure 12: Results from simulations of one beat of sinus rhythm in normal canine ventricular models. (A) Activation map simulated using the model with acquired fiber orientations (model 1). (B) Absolute difference between simulated activation maps obtained from a ventricular model with acquired fiber orientations and that with estimated fiber orientations, averaged over the five estimates. (C) Simulated pseudo-ECGs with models 1 and 3. (D) Simulated activation maps from ventricles with estimated fiber orientations (models 2-6).

Figure 13: Results from simulations of one beat of sinus rhythm in failing heart models. In the first column, rows 1-3 show activation maps calculated using models 7-9, respectively. In the second column, rows 1-3 display results of simulations with models 10-12, respectively. Rows 1-3 in the third column portray the absolute difference between the activation maps shown in the first and second columns of the corresponding row. Rows in the fourth column display simulated pseudo-ECGs from models in the first and second columns of the corresponding row.

Figure 14: Results from simulations of VT induction with the failing heart models. Rows 1-3 in the first column show activation maps during one cycle of reentrant activity in simulations with models 7-9, respectively. Rows 1-3 in the second column show activation maps corresponding to models 10-12, respectively. Rows in the third column illustrate pseudo-ECGs from models in the first and second columns of the corresponding row.

Discussion:

This research demonstrates quantitatively that, in the absence of DTMRI, myocardial fiber orientations of normal and failing ventricles can be estimated from in-vivo images of their geometries for use in simulations of cardiac electrophysiology. The proposed methodology is demonstrated with in vivo CT data, but it is equally applicable to in vivo MR images of ventricular geometry, addressing the lack of ability to directly acquire patient fiber orientations. It is thus an important step towards the development of personalized models of ventricular electrophysiology for clinical applications. The methodology can also be used to estimate the fiber orientations in ex-vivo hearts with high resolution. This is especially helpful when acquiring sub-millimeter resolution DTMRI images is difficult or prohibitively expensive, due to the very long acquisition times.

Our electrophysiological simulations suggested that activation maps were not very sensitive to changes in fiber orientations. More importantly, we demonstrated that effects of fiber estimation errors on gross electrophysiology were insignificant at a clinically observable level by means of the MAD score of the pseudo-ECGs. The MAD metric was suitable because it has been utilized in clinical studies, to compare ECGs of reentrant activity and paced propagation for localization of the organizing centers of reentrant circuits [29]. A MAD score of less than 12%, a threshold that our results satisfy, implies that the two underlying propagation patterns are

clinically equivalent. Note that the similarity of propagation patterns will translate to low differences in mechanical activation patterns as well, as reported experiments show that local electrical and mechanical activation times during sinus rhythm are highly correlated. In summary, our research will facilitate ventricular simulation studies of any species in health and disease when it is not feasible to acquire fiber orientations using DTMRI. In particular, the proposed methodology paves the way for patient-specific modeling of ventricular whole-heart electrophysiology (and possibly) electromechanics based only on in vivo clinical imaging data. Simulations with such models may ultimately aid physicians to arrive at highly personalized decisions for therapeutic interventions as well as prophylaxis. Incidentally, our results indicated that the performance of the proposed methodology was independent of the choice of the atlas. Accordingly, for the purposes of this study, a statistical atlas [17, 31] may not be required.

The current study has some limitations. Firstly, human heart image data were not available to us, and therefore the proposed estimation methodology was validated with images of canine hearts. We expect that the methodology will accurately estimate fiber orientations in human hearts as well because, just as in canine hearts, fiber orientations relative to geometry have been shown to be similar between different human hearts [17]. Also, we tested our methodology in normal and failing hearts only. It would be important to test it under conditions such as myocardial infarction and hypertrophy, where fiber disorganizations are known to occur [32, 33].

Disclosures:

We have nothing to disclose.

Acknowledgments:

We thank Drs. Raimond Winslow, Elliot McVeigh, and Patrick Helm at Johns Hopkins University for providing the ex vivo datasets online. This research was supported by National Institutes of Health grant R01-HL082729, and National Science Foundation grant CBET-0933029.

References:

[1] N. Trayanova, "Whole Heart Modeling: Applications to Cardiac Electrophysiology and Electromechanics," *Circulation Research,* vol. 108, no. pp. 113 - 128, 2011.

[2] F. Vadakkumpadan, H. Arevalo, C. Ceritoglu, M. Miller, and N. Trayanova, "Image-Based Estimation of Ventricular Fiber Orientations for Personalized Modeling of Cardiac Electrophysiology," *IEEE Transactions on Medical Imaging,* vol. 31, no. 5, pp. 1051 - 1060, 2012.

[3] F. Vadakkumpadan, V. Gurev, J. Constantino, H. Arevalo, and N. Trayanova, "Modeling of Whole-Heart Electrophysiology and Mechanics: Towards Patient-Specific

Simulations," in *Patient-Specific Modeling of the Cardiovascular System: Technology-Driven Personalized Medicine* R. Kerckhoffs, Ed., ed: Springer, 2010, pp. 145 - 165.

[4] A. E. Buxton, K. L. Lee, L. DiCarlo, M. R. Gold, G. S. Greer, E. N. Prystowsky, M. F. O'Toole, A. Tang, J. D. Fisher, J. Coromilas, M. Talajic, and G. Hafley, "Electrophysiologic testing to identify patients with coronary artery disease who are at risk for sudden death. Multicenter Unsustained Tachycardia Trial Investigators.," *The New England Journal of Medicine,* vol. 342, no. 26, pp. 1937 - 1945, 2000.

[5] D. Wei, O. Okazaki, K. Harumi, E. Harasawa, and H. Hosaka, "Comparative simulation of excitation and body surface electrocardiogram with isotropic and anisotropic computer heart models," *IEEE Transactions on Biomedical Engineering,* vol. 42, no. 4, pp. 343 - 357, 1995.

[6] L. J. Leon and B. M. Horacek, "Computer model of excitation and recovery in the anisotropic myocardium. II. Excitation in the simplified left ventricle," *Journal of Electrocardiology,* vol. 24, no. 1, pp. 17–31, 1991.

[7] D. Rohmer, A. Sitek, and G. T. Gullberg, "Reconstruction and Visualization of Fiber and Laminar Structure in the Normal Human Heart from Ex Vivo Diffusion Tensor Magnetic Resonance Imaging (DTMRI) Data," *Investigative Radiology,* vol. 42, no. 11, pp. 777 - 789, 2007.

[8] J. P. Daubert, W. Zareba, W. J. Hall, C. Schuger, A. Corsello, A. R. Leon, M. L. Andrews, S. McNitt, D. T. Huang, A. J. Moss, and M. I. S. Investigators., "Predictive value of ventricular arrhythmia inducibility for subsequent ventricular tachycardia or ventricular fibrillation in Multicenter Automatic Defibrillator Implantation Trial (MADIT) II patients.," *Journal of Americal College of Cardiology,* vol. 47, no. 1, pp. 98 - 107, 2006.

[9] D. E. Sosnovik, R. Wang, G. Dai, T. G. Reese, and V. J. Wedeen, "Diffusion MR tractography of the heart," *Journal of Cardiovascular Magnetic Resonance,* vol. 11, no. 1, pp. 47 - 61, 2009.

[10] H. Sundar, D. Shen, G. Biros, H. Litt, and C. Davatzikos, "Estimating myocardial fiber orientations by template warping," *Proc. IEEE International Symposium on Biomedical Imaging*, Arlington, VA, 2006, pp. 73 - 76.

[11] M. F. Beg, P. A. Helm, E. McVeigh, M. I. Miller, and R. L. Winslow, "Computational Cardiac Anatomy Using MRI," *Magnetic Resonance in Medicine,* vol. 52, no. 5, pp. 1167 - 1174, 2004.

[12] D. C. Alexander, C. Pierpaoli, P. J. Basser, and J. C. Gee, "Spatial Transformations of Diffusion Tensor Magnetic Resonance Images," *IEEE Transactions on Medical Imaging,* vol. 20, no. 11, pp. 1131 - 1139, 2001.

[13] P. A. Helm, L. Younes, M. F. Beg, D. B. Ennis, C. Leclercq, O. P. Faris, E. McVeigh, D. Kass, M. I. Miller, and R. L. Winslow, "Evidence of Structural Remodeling in the Dyssynchronous Failing Heart," *Circulation Research,* vol. 98, no. 1, pp. 125 - 132, 2006.

[14] P. Helm, M. F. Beg, M. Miller, and R. Winslow, "Measuring and mapping cardiac fiber and laminar architecture using diffusion tensor MR imaging," *Annals of the New York Academy of Sciences,* vol. 1047, no. pp. 296 - 307, 2005.

[15] P. A. Helm, H.-J. Tseng, L. Younes, E. R. McVeigh, and R. L. Winslow, "Ex vivo 3D diffusion tensor imaging and quantification of cardiac laminar structure," *Magnetic Resonance in Imaging,* vol. 54, no. 4, pp. 850 - 859, 2005.

[16] D. F. Scollan, A. Holmes, R. Winslow, and J. Forder, "Histological validation of myocardial microstructure obtained from diffusion tensor magnetic resonance imaging," *American Journal of Physiology - Heart and Circulatory Physiology,* vol. 275, no. 6, pp. H2308 - H2318, 1998.

[17] H. Lombaert, J. Peyrat, P. Croisille, S. Rapacchi, L. Fanton, F. Cheriet, P. Clarysse, I. Magnin, H. Delingette, and N. Ayache, "Human Atlas of the Cardiac Fiber Architecture: Study on a Healthy Population," *IEEE Transactions on Medical Imaging,* vol. 31, no. 7, pp. 1436 - 1447, 2012.

[18] D. D. Streeter, *Gross morphology and fiber geometry of the heart*. Baltimore: Johns Hopkins Press, 1979.

[19] F. Vadakkumpadan, H. Arevalo, A. J. Prassl, J. Chen, F. Kickinger, P. Kohl, G. Plank, and N. Trayanova, "Image-based models of cardiac structure in health and disease," *Wiley Interdisciplinary Reviews: Systems Biology and Medicine,* vol. 2, no. 4, pp. 489 - 506, 2010.

[20] F. Vadakkumpadan, L. J. Rantner, B. Tice, P. Boyle, A. J. Prassl, E. Vigmond, G. Plank, and N. Trayanova, "Image-Based Models of Cardiac Structure with Applications in Arrhythmia and Defibrillation Studies," *Journal of Electrocardiology,* vol. 42, no. 2, pp. 157.e1 - 157.e10, 2009.

[21] G. Plank, L. Zhou, J. L. Greenstein, G. Plank, L. Zhou, J. L. Greenstein, S. Cortassa, R. L. Winslow, B. O'Rourke, and N. A. Trayanova, "From mitochondrial ion channels to arrhythmias in the heart: computational techniques to bridge the spatio-temporal scales," *Philosophical Transactions Series A, Mathematical, Physical, and Engineering Sciences,* vol. 366, no. 1879, pp. 3381-3409, 2008.

[22] D. E. Roberts and A. M. Scher, "Effect of tissue anisotropy on extracellular potential fields in canine myocardium in situ," *Circulation Research,* vol. 50, no. pp. 342 - 351, 1982.

[23] J. Greenstein, R. Wu, S. Po, G. F. Tomaselli, and R. L. Winslow, "Role of the Calcium-Independent Transient Outward Current I(to1) in Shaping Action Potential Morphology and Duration," *Circulation Research,* vol. 87, no. pp. 1026 - 1033, 2000.

[24] R. Winslow, J. Rice, S. Jafri, E. Marbán, and B. O'Rourke, "Mechanisms of altered excitation-contraction coupling in canine tachycardia-induced heart failure, II: model studies," *Circulation Research,* vol. 84, no. 5, pp. 571 - 586, 1999.

[25] F. Akar, R. Nass, S. Hahn, E. Cingolani, M. Shah, G. Hesketh, D. DiSilvestre, R. Tunin, D. Kass, and G. Tomaselli, "Dynamic Changes in Conduction Velocity and Gap Junction Properties During Development of Pacing-Induced Heart Failure," *American Journal of Physiology - Heart and Circulatory Physiology,* vol. 293, no. 2, pp. H1223 - H1230, 2007.

[26] V. Gurev, J. Constantino, J. J. Rice, and N. Trayanova, "Distribution of Electromechanical Delay in the Ventricles:Insights from a 3D Electromechanical Model of the Heart," *Biophysical Journal,* vol. 99, no. 3, pp. 745-754, 2010.

[27] K. H. W. J. t. Tusscher, R. Hren, and A. V. Panfilov, "Organization of Ventricular Fibrillation in the Human Heart," *Circulation Research,* vol. 100, no. 12, pp. e87 - e101, 2007.

[28] K. Gima and Y. Rudy, "Ionic Current Basis of Electrocardiographic Waveforms," *Circulation Research,* vol. 90, no. 8, pp. 889 - 896, 2002.

[29] E. Gerstenfeld, S. Dixit, D. Callans, Y. Rajawat, R. Rho, and F. Marchlinski, "Quantitative comparison of spontaneous and paced 12-lead electrocardiogram during right ventricular outflow tract ventricular tachycardia," *Journal of Americal College of Cardiology,* vol. 41, no. 11, pp. 2046 - 2053, 2003.

[30] M. Potse, B. Dube, J. Richer, A. Vinet, and R. M. Gulrajani, "A comparison of monodomain and bidomain reaction-diffusion models for action potential propagation in the human heart," *IEEE Transactions on Biomedical Engineering,* vol. 53, no. 12, pp. 2425 - 2435, 2006.

[31] J.-M. Peyrat, M. Sermesant, X. Pennec, H. Delingette, X. Chenyang, E. R. McVeigh, and N. Ayache, "A Computational Framework for the Statistical Analysis of Cardiac Diffusion Tensors: Application to a Small Database of Canine Hearts," *IEEE Transactions on Medical Imaging,* vol. 26, no. 11, pp. 1500 - 1514, 2007.

[32] J. Chen, S.-K. Song, W. Liu, M. McLean, S. J. Allen, J. Tan, S. A. Wickline, and X. Yu, "Remodeling of cardiac fiber structure after infarction in rats quantified with diffusion tensor MRI," *American Journal of Physiology - Heart and Circulatory Physiology,* vol. 285, no. 3, pp. H946-954, 2003.

[33] E. C. Stecker and S. S. Chugh, "Prediction of sudden cardiac death: next steps in pursuit of effective methodology," *Journal of Interventional Cardiac Electrophysiology,* vol. 31, no. 2, pp. 101 - 107, 2011.

1

Click here to download high resolution image

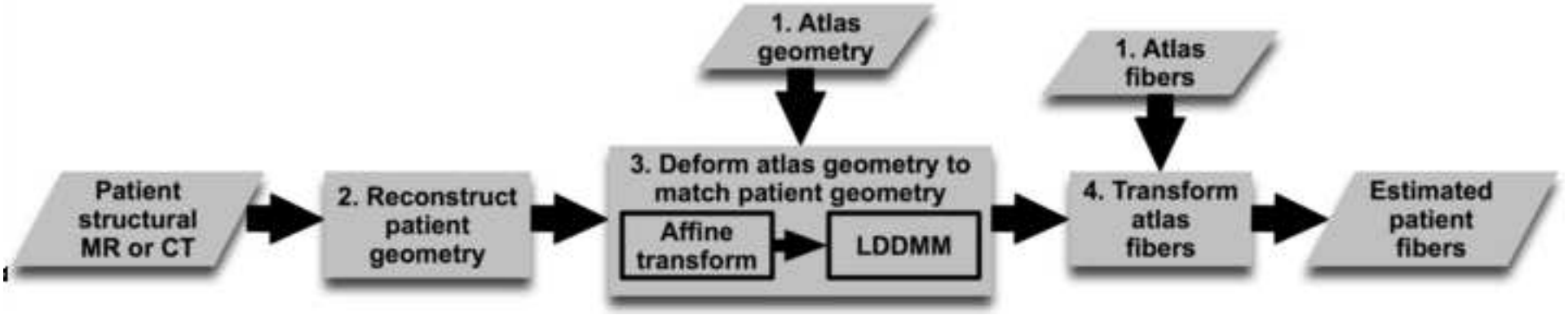

2
Click here to download high resolution image

3
Click here to download high resolution image

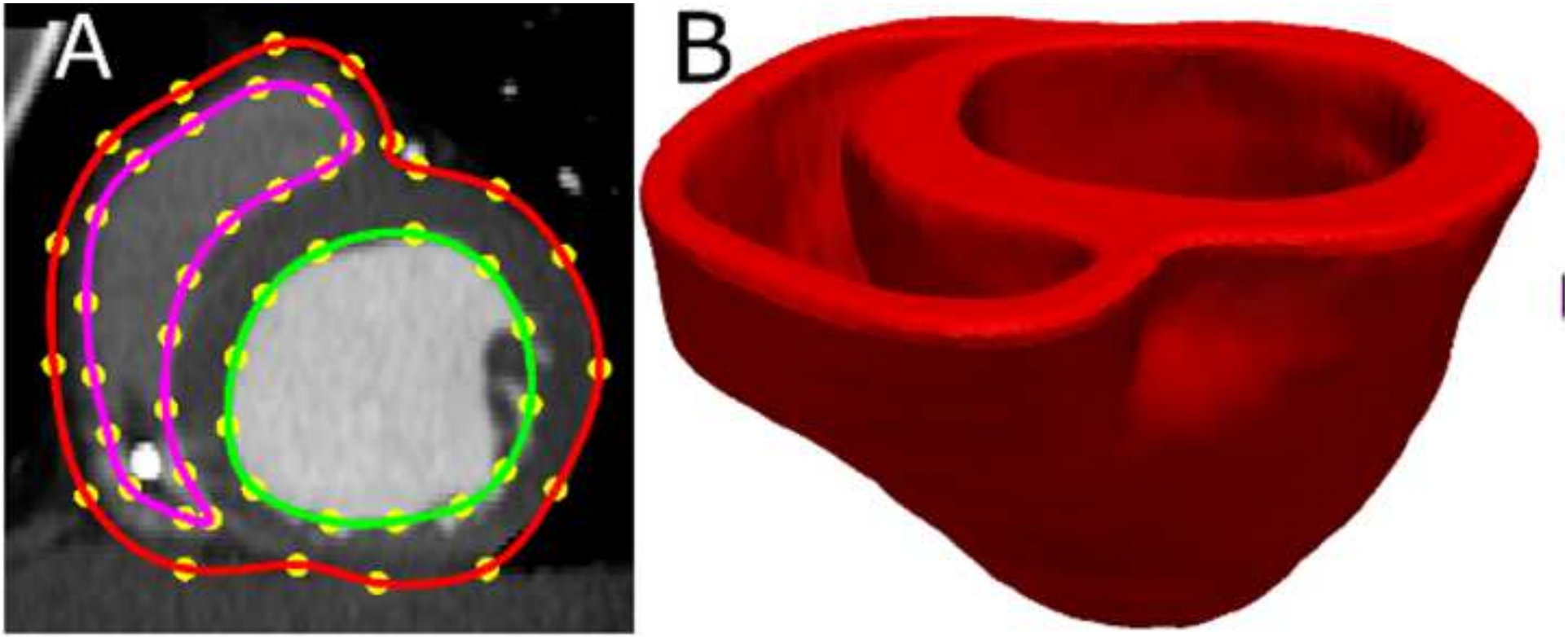

Click here to download high resolution image

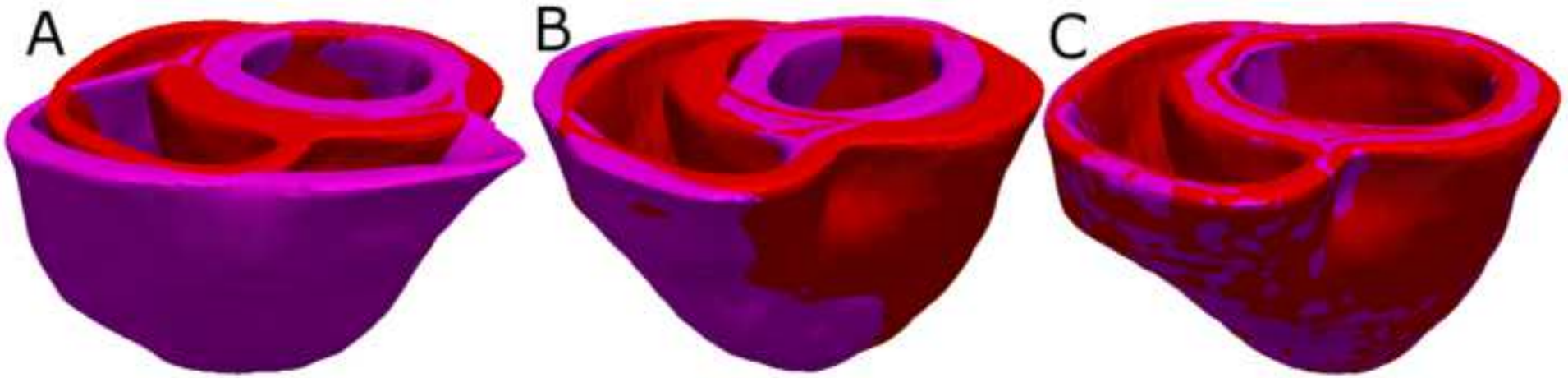

5

Click here to download high resolution image

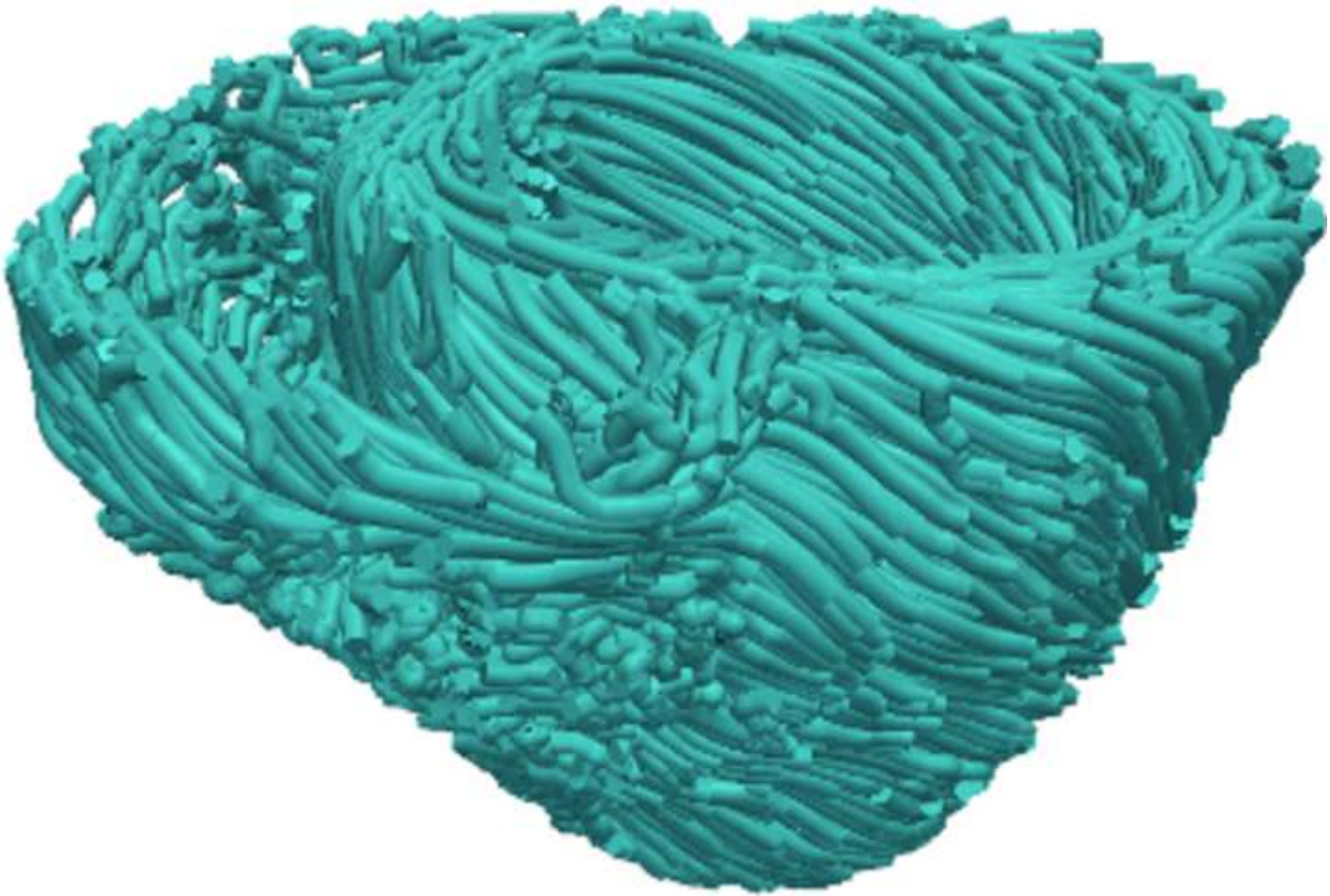

6
Click here to download high resolution image

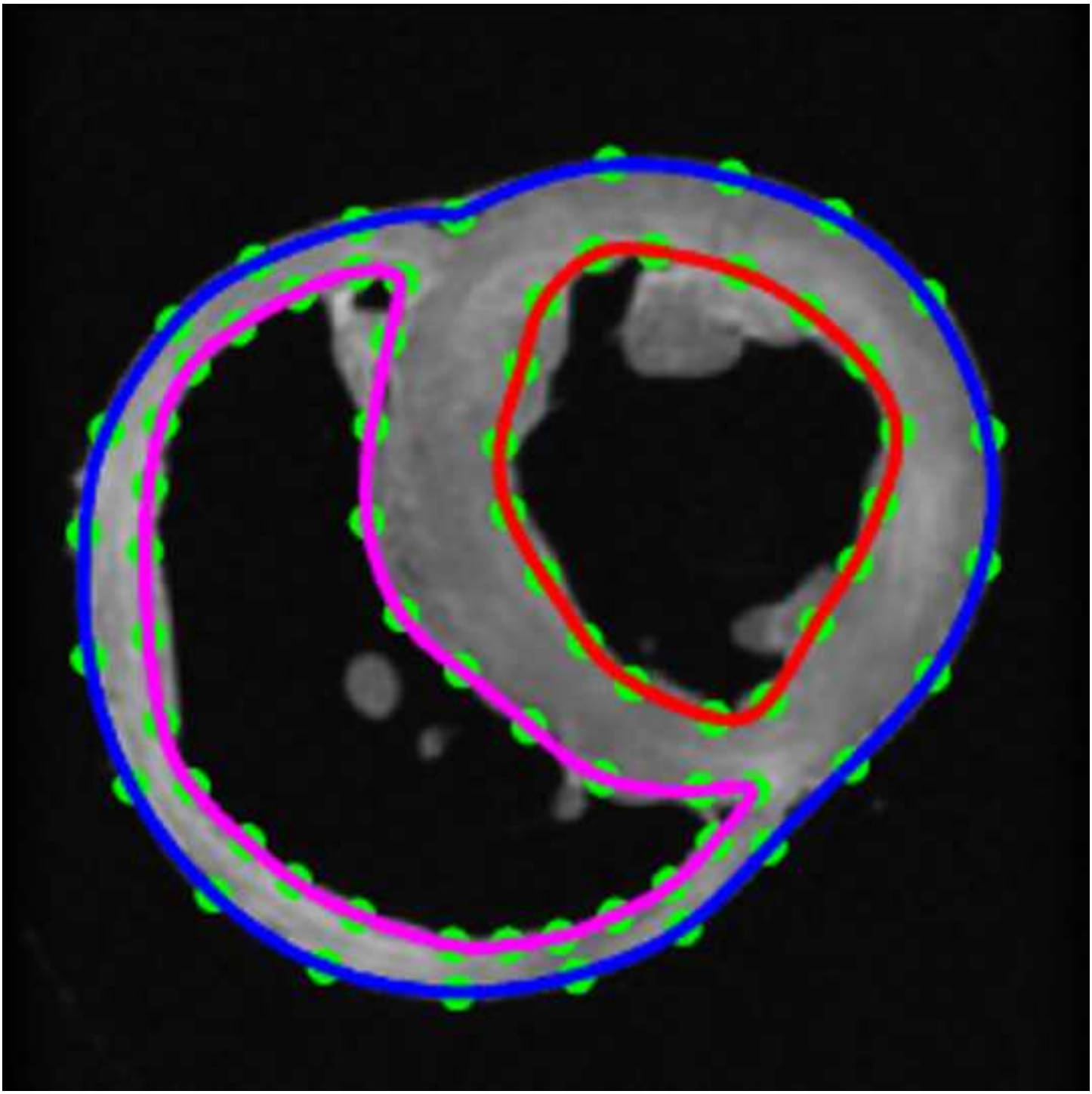

Click here to download high resolution image

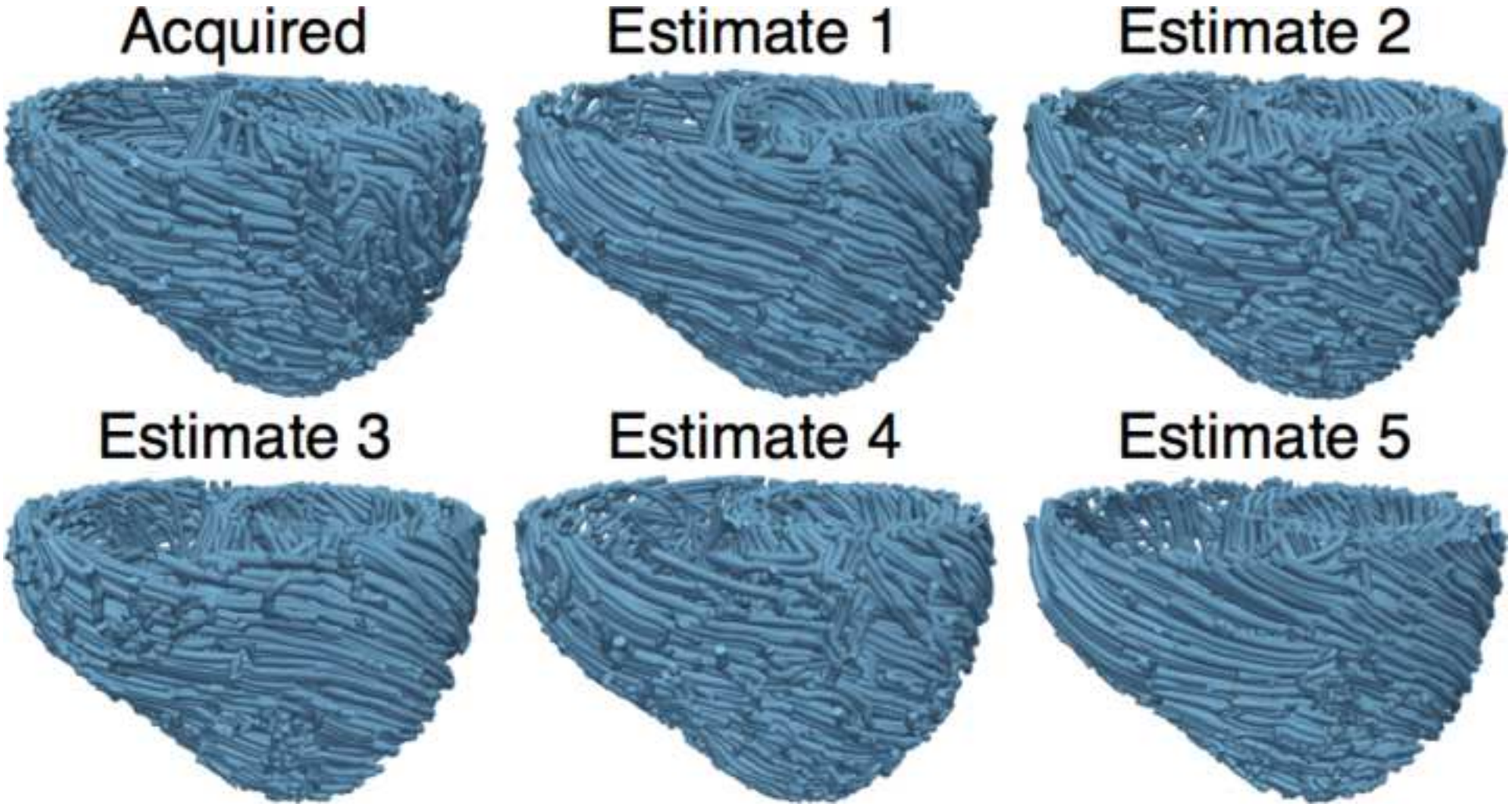

Click here to download high resolution image

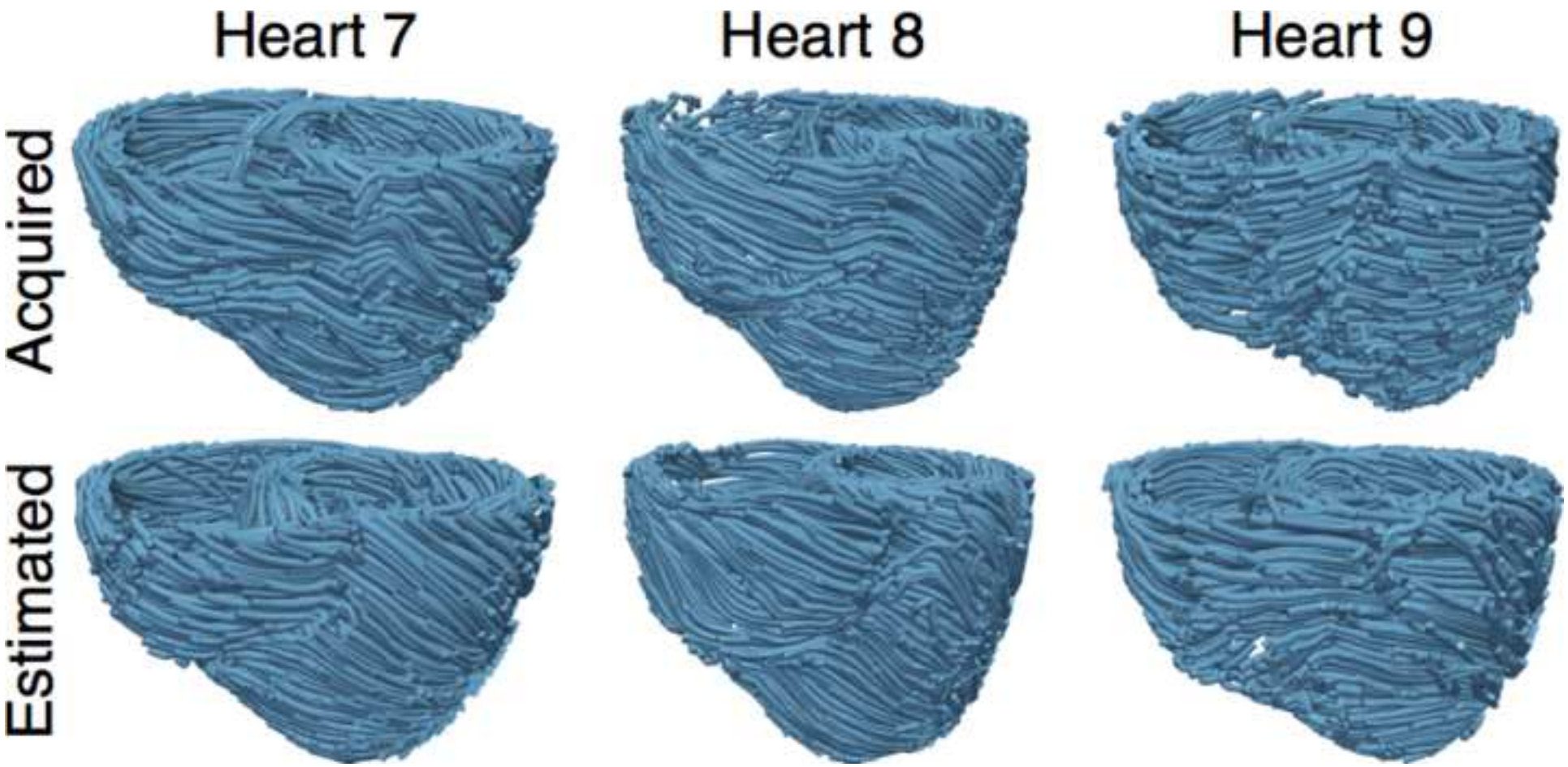

Click here to download high resolution image

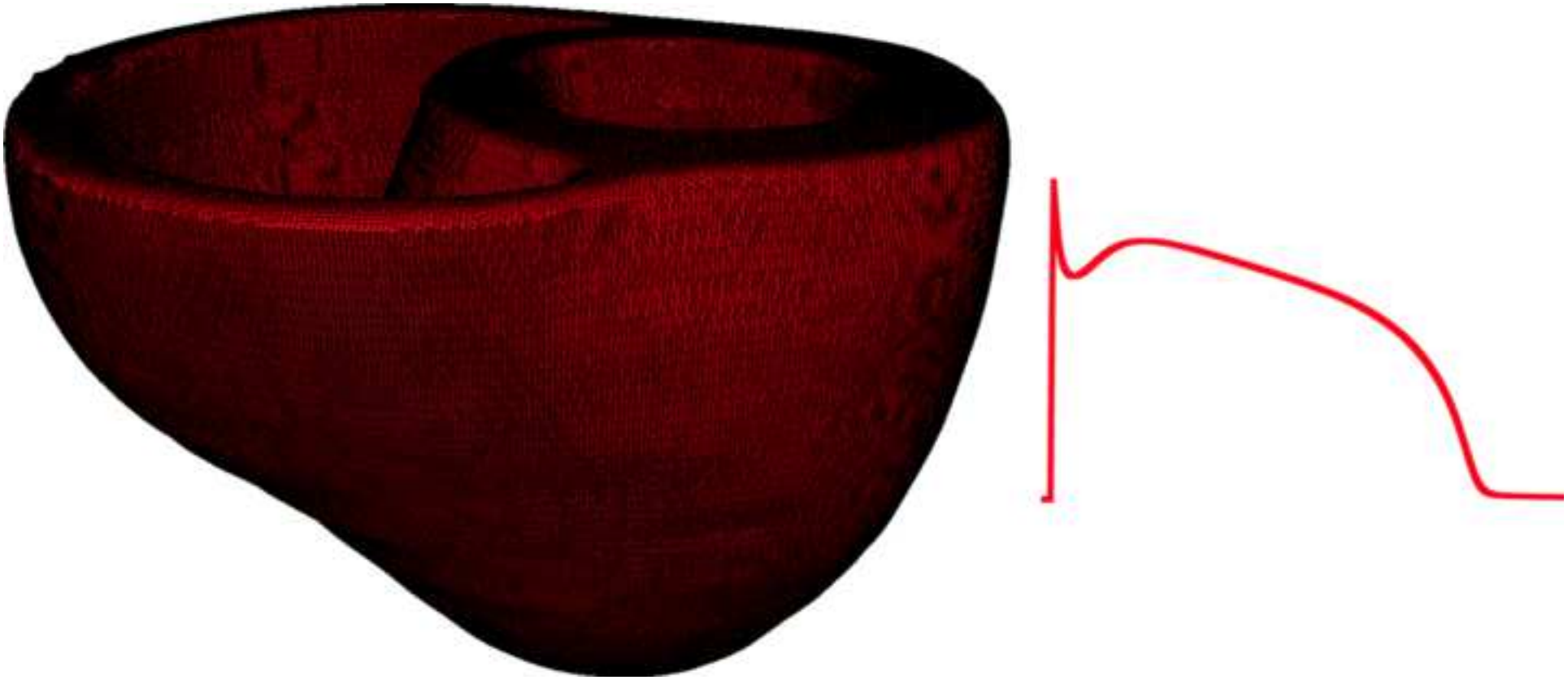

Click here to download high resolution image

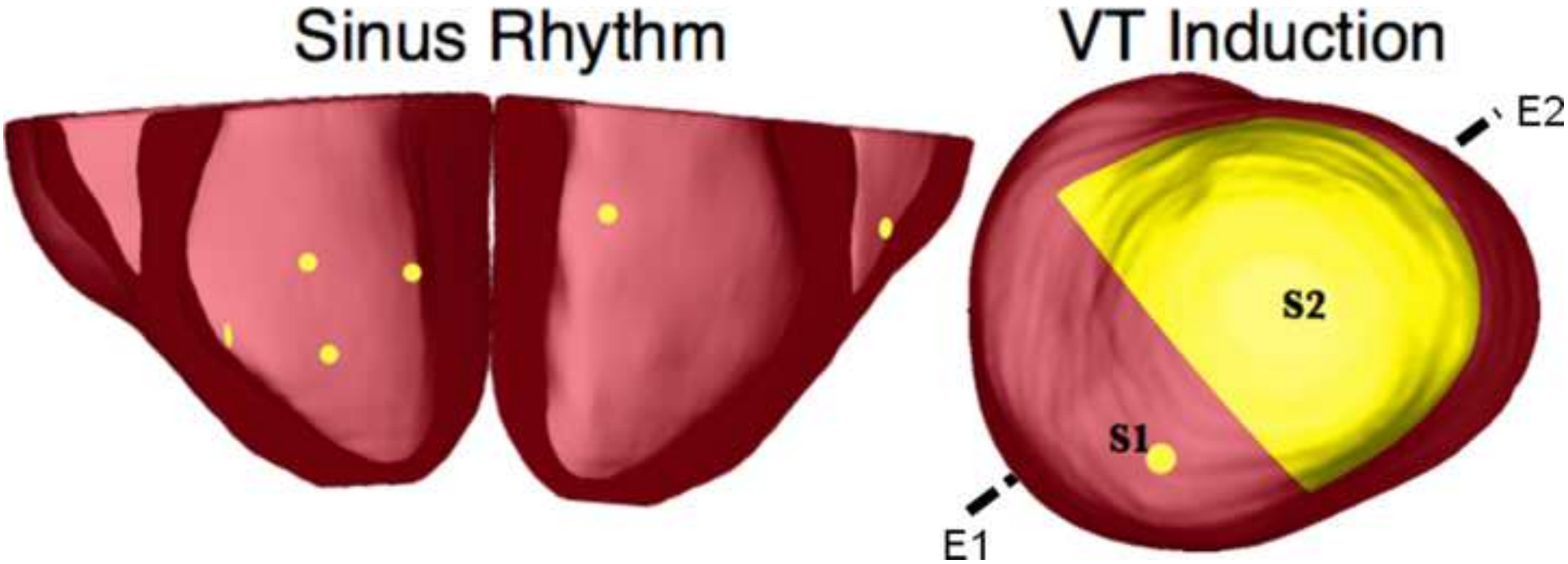

Click here to download high resolution image

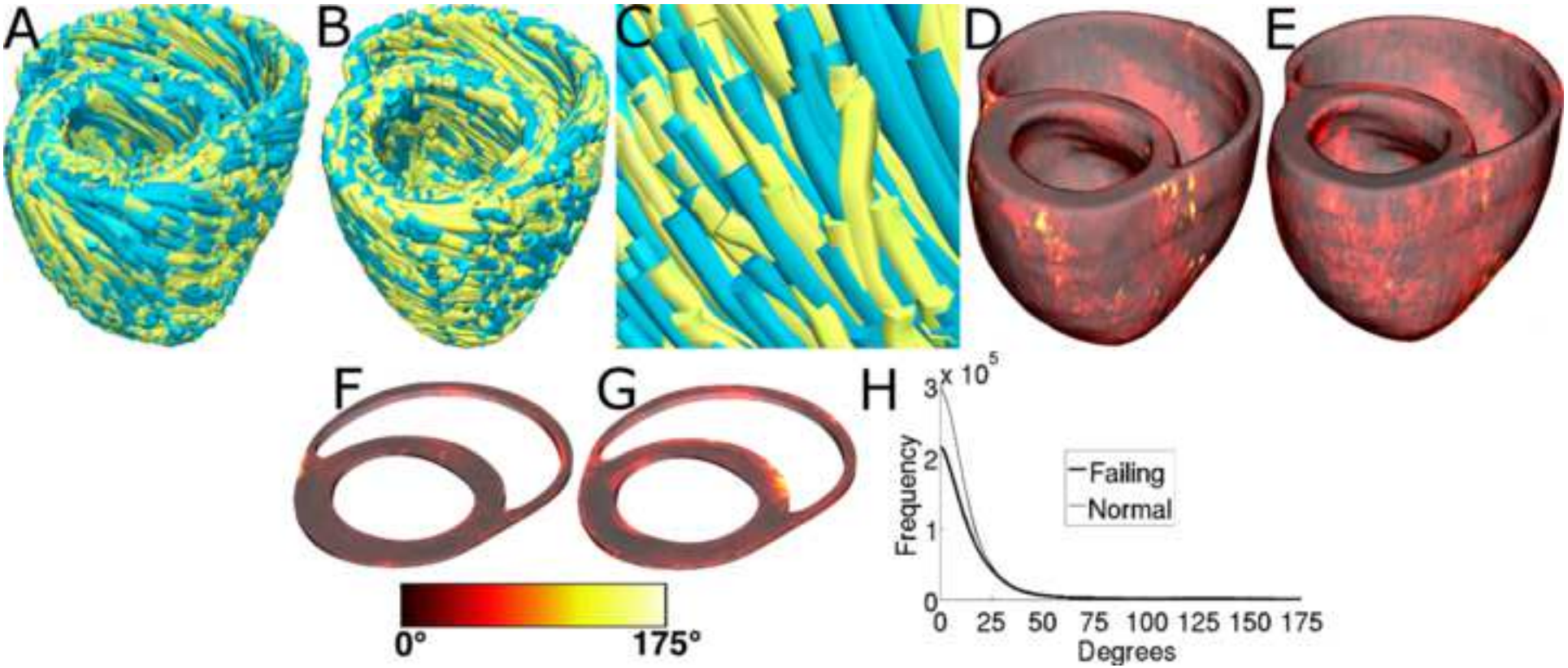

Click here to download high resolution image

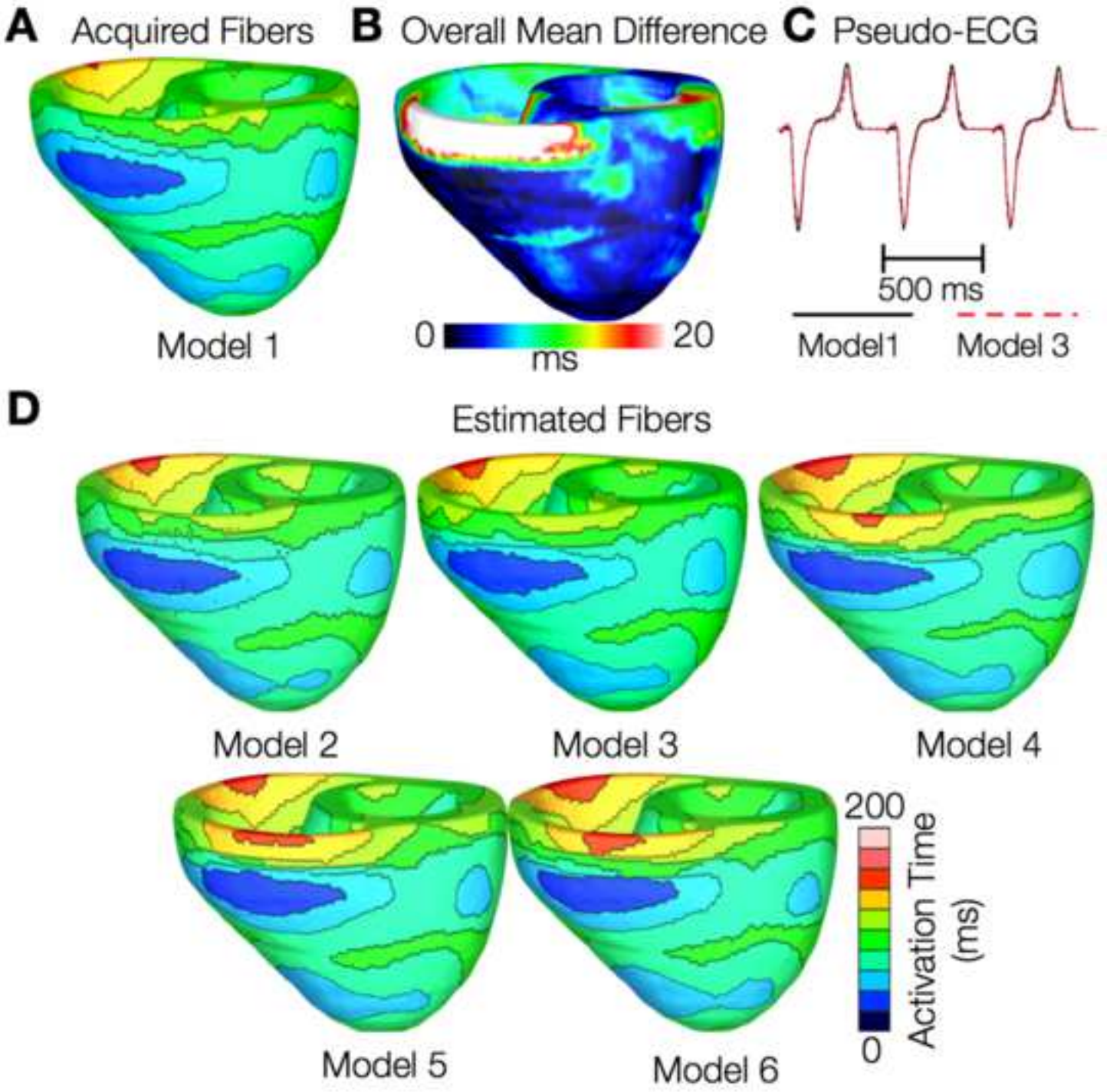

Click here to download high resolution image

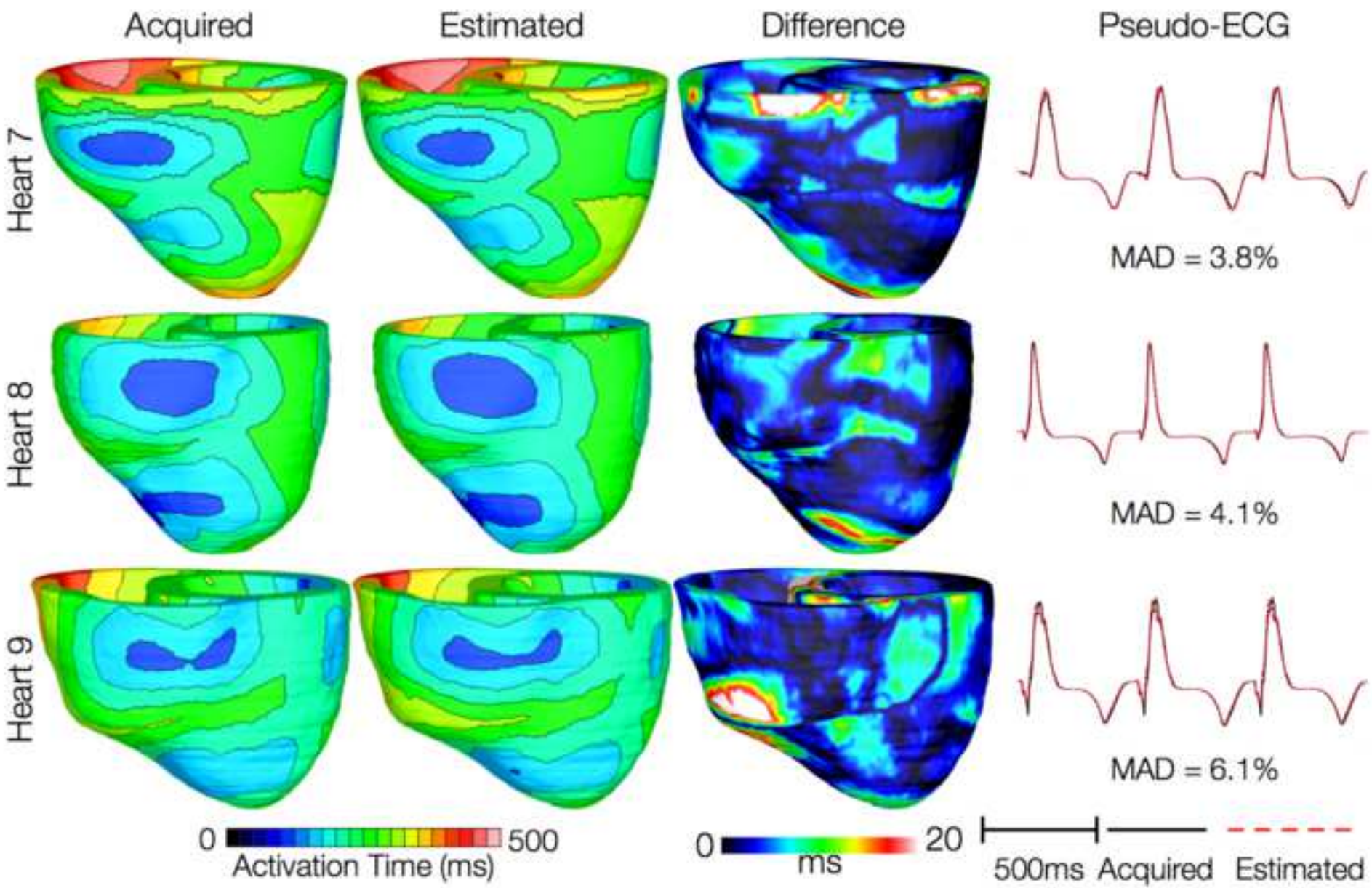

Click here to download high resolution image

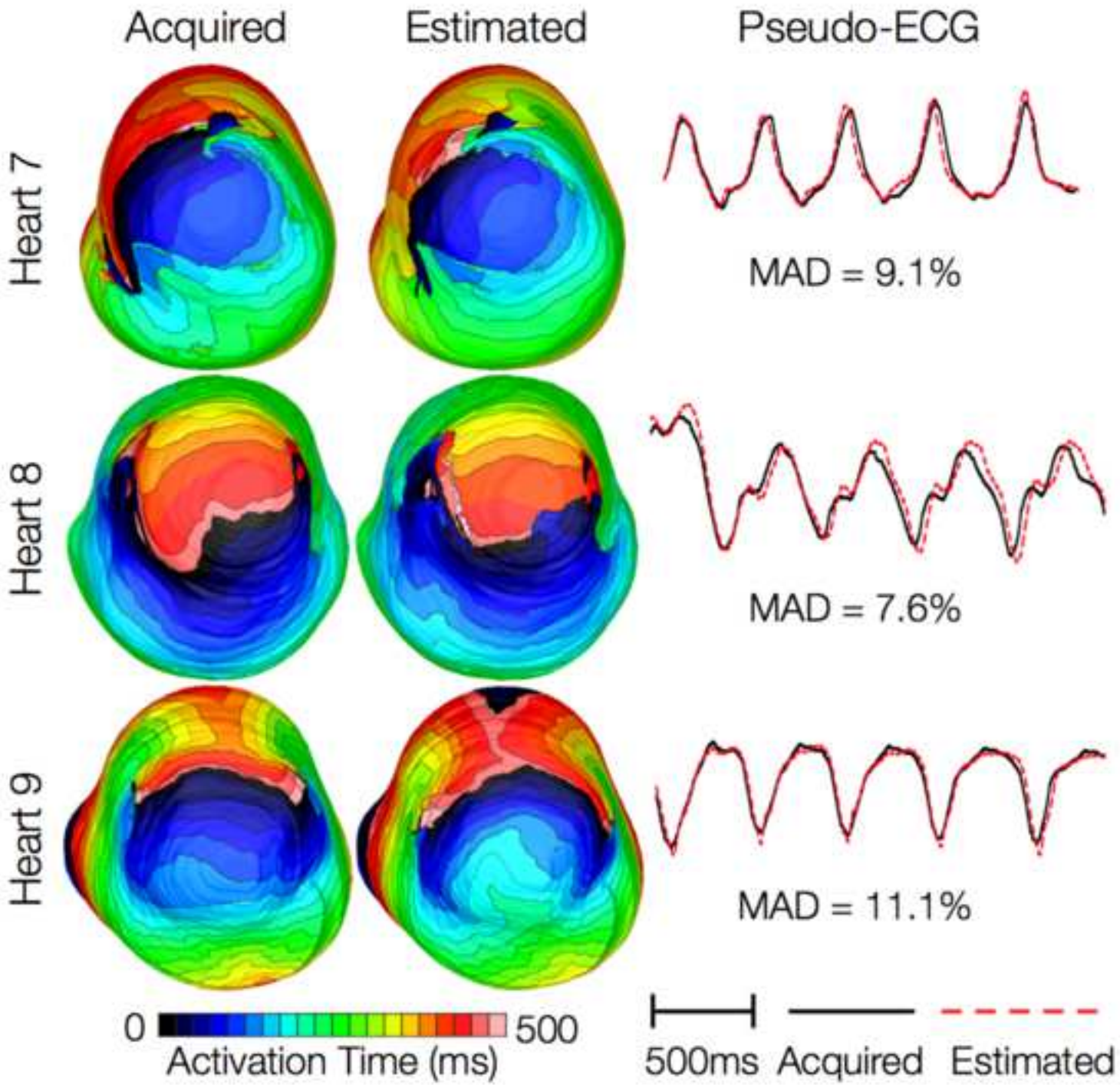

*Table of Reagents/ Materials Used

Click here to download Table of Reagents/ Materials Used: equipment.xlsx

Equipment/Software/Data	Company	Catalog Number
Desktop workstations	Xi Computers	Custom order
LDDMM	Johns Hopkins University	NA
MATLAB	Mathworks, Inc.	R2011b
ImageJ	National Institutes of Health	NA
Tarantula	CAE Software Solutions	NA
CARP	CardioSolv	NA
Canine images	Johns Hopkins University	NA

Comments

Quad-core AMD Opteron processor, 8-32GB RAM. Website: http://www.xicomputer.com/

Website: http://cis.jhu.edu/software/lddmm-volume/index.php

Website: http://www.mathworks.com/products/matlab/

Source: http://rsbweb.nih.gov/ij/

Website: http://www.meshing.at/Spiderhome/Tarantula.html

http://cardiosolv.com/

Source: http://www.ccbm.jhu.edu/research/DTMRIDS.php

jove JOURNAL OF VISUALIZED EXPERIMENTS
17 Sellers Street
Cambridge, MA 02139
tel. +1.617.945.9051
www.JoVE.com

ARTICLE AND VIDEO LICENSE AGREEMENT

Manuscript #:

Title of Article: Patient-Specific Modeling of the Heart: Estimation of Ventricular Fiber Orientations

Author(s): Fijoy Vadakkumpadan, Hermenegild Arevalo, Natalia Trayanova

Item 1 (check one box): The Author elects to have the Materials be made available (as described at http://www.jove.com/publish) via: ☑ Standard Access ☐ Open Access

Item 2 (check one box):

☑ The Author is NOT a United States government employee.

☐ The Author is a United States government employee and the Materials were prepared in the course of his or her duties as a United States government employee.

☐ The Author is a United States government employee but the Materials were NOT prepared in the course of his or her duties as a United States government employee.

ARTICLE AND VIDEO LICENSE AGREEMENT

1. Defined Terms. As used in this Article and Video License Agreement, the following terms shall have the following meanings: "**Agreement**" means this Article and Video License Agreement; "**Article**" means the article specified on the last page of this Agreement, including any associated materials such as texts, figures, tables, artwork, abstracts, or summaries contained therein; "**Author**" means the author who is a signatory to this Agreement; "**Collective Work**" means a work, such as a periodical issue, anthology or encyclopedia, in which the Materials in their entirety in unmodified form, along with a number of other contributions, constituting separate and independent works in themselves, are assembled into a collective whole; "**CRC License**" means the Creative Commons Attribution-Non Commercial-No Derivs 3.0 Unported Agreement, the terms and conditions of which can be found at: http://creativecommons.org/licenses/by-nc-nd/3.0/legalcode; "**Derivative Work**" means a work based upon the Materials or upon the Materials and other pre-existing works, such as a translation, musical arrangement, dramatization, fictionalization, motion picture version, sound recording, art reproduction, abridgment, condensation, or any other form in which the Materials may be recast, transformed, or adapted; "**Institution**" means the institution, listed on the last page of this Agreement, by which the Author was employed at the time of the creation of the Materials; "**JoVE**" means MyJove Corporation, a Massachusetts corporation and the publisher of *The Journal of Visualized Experiments*; "**Materials**" means the Article and / or the Video; "**Parties**" means the Author and JoVE; "**Video**" means any video(s) made by the Author, alone or in conjunction with any other parties, or by JoVE or its affiliates or agents, individually or in collaboration with the Author or any other parties, incorporating all or any portion of the Article, and in which the Author may or may not appear.

2. Background. The Author, who is the author of the Article, in order to ensure the dissemination and protection of the Article, desires to have the JoVE publish the Article and create and transmit videos based on the Article. In furtherance of such goals, the Parties desire to memorialize in this Agreement the respective rights of each Party in and to the Article and the Video.

3. Grant of Rights in Article. In consideration of JoVE agreeing to publish the Article, the Author hereby grants to JoVE, subject to **Sections 4** and **7** below, the exclusive, royalty-free, perpetual (for the full term of copyright in the Article, including any extensions thereto) license (a) to publish, reproduce, distribute, display and store the Article in all forms, formats and media whether now known or hereafter developed (including without limitation in print, digital and electronic form) throughout the world, (b) to translate the Article into other languages, create adaptations, summaries or extracts of the Article or other Derivative Works (including, without limitation, the Video) or Collective Works based on all or any portion of the Article and exercise all of the rights set forth in (a) above in such translations, adaptations, summaries, extracts, Derivative Works or Collective Works and (c) to license others to do any or all of the above. The foregoing rights may be exercised in all media and formats, whether now known or hereafter devised, and include the right to make such modifications as are technically necessary to exercise the rights in other media and formats. If the "Open Access" box has been checked in **Item 1** above, JoVE and the Author hereby grant to the public all such rights in the Article

as provided in, but subject to all limitations and requirements set forth in, the CRC License.

4. Retention of Rights in Article. Notwithstanding the exclusive license granted to JoVE in **Section 3** above, the Author shall, with respect to the Article, retain the non-exclusive right to use all or part of the Article for the non-commercial purpose of giving lectures, presentations or teaching classes, and to post a copy of the Article on the Institution's website or the Author's personal website, in each case provided that a link to the Article on the JoVE website is provided and notice of JoVE's copyright in the Article is included. All non-copyright intellectual property rights in and to the Article, such as patent rights, shall remain with the Author.

5. Grant of Rights in Video – Standard Access. This **Section 5** applies if the "Standard Access" box has been checked in **Item 1** above or if no box has been checked in **Item 1** above. In consideration of JoVE agreeing to produce, display or otherwise assist with the Video, the Author hereby acknowledges and agrees that, Subject to **Section 7** below, JoVE is and shall be the sole and exclusive owner of all rights of any nature, including, without limitation, all copyrights, in and to the Video. To the extent that, by law, the Author is deemed, now or at any time in the future, to have any rights of any nature in or to the Video, the Author hereby disclaims all such rights and transfers all such rights to JoVE.

6. Grant of Rights in Video – Open Access. This **Section 6** applies only if the "Open Access" box has been checked in **Item 1** above. In consideration of JoVE agreeing to produce, display or otherwise assist with the Video, the Author hereby grants to JoVE, subject to **Section 7** below, the exclusive, royalty-free, perpetual (for the full term of copyright in the Article, including any extensions thereto) license (a) to publish, reproduce, distribute, display and store the Video in all forms, formats and media whether now known or hereafter developed (including without limitation in print, digital and electronic form) throughout the world, (b) to translate the Video into other languages, create adaptations, summaries or extracts of the Video or other Derivative Works or Collective Works based on all or any portion of the Video and exercise all of the rights set forth in (a) above in such translations, adaptations, summaries, extracts, Derivative Works or Collective Works and (c) to license others to do any or all of the above. The foregoing rights may be exercised in all media and formats, whether now known or hereafter devised, and include the right to make such modifications as are technically necessary to exercise the rights in other media and formats. For any Video to which this Section 6 is applicable, JoVE and the Author hereby grant to the public all such rights in the Video as provided in, but subject to all limitations and requirements set forth in, the CRC License.

7. Government Employees. If the Author is a United States government employee and the Article was prepared in the course of his or her duties as a United States government employee, as indicated in **Item 2** above, and any of the licenses or grants granted by the Author hereunder exceed the scope of the 17 U.S.C. 403, then the rights granted hereunder shall be limited to the maximum rights permitted under such statute. In such case, all provisions contained herein that are not in conflict with such statute shall remain in full force and effect, and all provisions contained herein that do so conflict shall be deemed to be amended so as to provide to JoVE the maximum rights permissible within such statute.

8. Likeness, Privacy, Personality. The Author hereby grants JoVE the right to use the Author's name, voice, likeness, picture, photograph, image, biography and performance in any way, commercial or otherwise, in connection with the Materials and the sale, promotion and distribution thereof. The Author hereby waives any and all rights he or she may have, relating to his or her appearance in the Video or otherwise relating to the Materials, under all applicable privacy, likeness, personality or similar laws.

9. Author Warranties. The Author represents and warrants that the Article is original, that it has not been published, that the copyright interest is owned by the Author (or, if more than one author is listed at the beginning of this Agreement, by such authors collectively) and has not been assigned, licensed, or otherwise transferred to any other party. The Author represents and warrants that the author(s) listed at the top of this Agreement are the only authors of the Materials. If more than one author is listed at the top of this Agreement and if any such author has not entered into a separate Article and Video License Agreement with JoVE relating to the Materials, the Author represents and warrants that the Author has been authorized by each of the other such authors to execute this Agreement on his or her behalf and to bind him or her with respect to the terms of this Agreement as if each of them had been a party hereto as an Author. The Author warrants that the use, reproduction, distribution, public or private performance or display, and/or modification of all or any portion of the Materials does not and will not violate, infringe and/or misappropriate the patent, trademark, intellectual property or other rights of any third party. The Author represents and warrants that it has and will continue to comply with all government, institutional and other regulations, including, without limitation all institutional, laboratory, hospital, ethical, human and animal treatment, privacy, and all other rules, regulations, laws, procedures or guidelines, applicable to the Materials, and that all research involving human and animal subjects has been approved by the Author's relevant institutional review board.

10. JoVE Discretion. If the Author requests the assistance of JoVE in producing the Video in the Author's facility, the Author shall ensure that the presence of JoVE employees, agents or independent contractors is in accordance with the relevant regulations of the Author's institution. If more than one author is listed at the beginning of this Agreement, JoVE may, in its sole discretion, elect not take any action with respect to the Article until such time as it has received complete, executed Article and Video License Agreements from each such author. JoVE reserves the right, in its absolute and sole discretion and without giving any reason therefore, to accept or decline any work submitted to JoVE. JoVE and its

jove JOURNAL OF VISUALIZED EXPERIMENTS
17 Sellers Street
Cambridge, MA 02139
tel. +1.617.945.9051
www.JoVE.com

ARTICLE AND VIDEO LICENSE AGREEMENT

employees, agents and independent contractors shall have full, unfettered access to the facilities of the Author or of the Author's institution as necessary to make the Video, whether actually published or not. JoVE has sole discretion as to the method of making and publishing the Materials, including, without limitation, to all decisions regarding editing, lighting, filming, timing of publication, if any, length, quality, content and the like.

11. Indemnification. The Author agrees to indemnify JoVE and/or its successors and assigns from and against any and all claims, costs, and expenses, including attorney's fees, arising out of any breach of any warranty or other representations contained herein. The Author further agrees to indemnify and hold harmless JoVE from and against any and all claims, costs, and expenses, including attorney's fees, resulting from the breach by the Author of any representation or warranty contained herein or from allegations or instances of violation of intellectual property rights, damage to the Author's or the Author's institution's facilities, fraud, libel, defamation, research, equipment, experiments, property damage, personal injury, violations of institutional, laboratory, hospital, ethical, human and animal treatment, privacy or other rules, regulations, laws, procedures or guidelines, liabilities and other losses or damages related in any way to the submission of work to JoVE, making of videos by JoVE, or publication in *JoVE* or elsewhere by JoVE. The Author shall be responsible for, and shall hold JoVE harmless from, damages caused by lack of sterilization, lack of cleanliness or by contamination due to the making of a video by JoVE its employees, agents or independent contractors. All sterilization, cleanliness or decontamination procedures shall be solely the responsibility of the Author and shall be undertaken at the Author's expense. All indemnifications provided herein shall include JoVE's attorney's fees and costs related to said losses or damages. Such indemnification and holding harmless shall include such losses or damages incurred by, or in connection with, acts or omissions of JoVE, its employees, agents or independent contractors.

12. Fees. To cover the cost incurred for publication, JoVE must receive payment before production and publication the Materials. Payment is due in 21 days of invoice. Should the Materials not be published due to an editorial or production decision, these funds will be returned to the Author. Withdrawal by the Author of any submitted Materials after final peer review approval will result in a US$1,200 fee to cover pre-production expenses incurred by JoVE. If payment is not received by the completion of filming, production and publication of the Materials will be suspended until payment is received.

13. Transfer, Governing Law. This Agreement may be assigned by JoVE and shall inure to the benefits of any of JoVE's successors and assignees. This Agreement shall be governed and construed by the internal laws of the Commonwealth of Massachusetts without giving effect to any conflict of law provision thereunder. This Agreement may be executed in counterparts, each of which shall be deemed an original, but all of which together shall be deemed to me one and the same agreement. A signed copy of this Agreement delivered by facsimile, e-mail or other means of electronic transmission shall be deemed to have the same legal effect as delivery of an original signed copy of this Agreement.

A signed copy of this document must be sent with all new submissions.

AUTHOR:

Name: Fijoy Vadakkumpadan

Department: Biomedical Engineering

Institution: Johns Hopkins University

Article Title: Patient-Specific Modeling of the Heart: Estimation of Ventricular Fiber Orientations

Signature: [signature] Date: 6-1-2012

Please submit a signed and dated copy of this license by one of the following three methods:

1) Upload a scanned copy of the document as a pfd on the JoVE submission site;
2) Fax the document to +1.866.381.2236; or
3) Mail the document to JoVE / Attn: JoVE Editorial / 17 Sellers St / Cambridge, MA 02139

For questions, please email editorial@jove.com or call +1.617.945.9051.

*Rebuttal Comments
Click here to download Rebuttal Comments: reviewerComments.docx

Reviewer #1:

Summary:

The authors present an interesting and highly relevant method which is an important processing step in any endeavor that aims at applying in-silico modeling of cardiac function to address clinical questions. Fiber orientation plays a key role in determining cardiac activation and repolarization sequences and as such the proposed method is of great interest to communities such as the cardiac Physiome community which focuses on clinical aspects of cardiac modeling. In my view, the method is sound and well presented. My main concerns relate to some parameter choices and the lack of quantitative comparisons of simulation results with experimental data, only comparisons between simulation results obtained with measured versus estimated fiber arrangements are made. Another issue is the incomplete comparison with other methods which have been applied previously for the same purposes such as rule-based techniques, as they are being used by the authors themselves (see, for instance, Bayer et al, Ann. Biomed. Eng. 2012). These issues have to be addressed before the manuscript can be accepted for publication.

- We thank the review for his/her time reviewing our manuscript and valuable feedback. The purpose of this paper is not to validate simulation results with experimental data; this has been done in extensive work by Dr. Trayanova's team and others. Rather, as stated in the Introduction section, the objective here is to propose a new methodology to estimate ventricular fiber orientations, and show that the estimated fiber orientations are as good as a physiologically accurate measurement (DTMRI). The methodology and results described in this JoVE article have been thoroughly reviewed and published by IEEE Transactions on Medical Imaging (IEEE-TMI) journal (see reference [3]), where a more detailed description of parameters as well as comparison with existing methods is available. As per instructions from the editorial office, this JoVE article focuses on "how" to perform the estimation and "how" to validate the estimate, in order to disseminate previously accepted and published methodologies in the video format. Please see below for out point-by-point responses to specific comments.

Major Concerns:

The choice of conductivities in the computer model is quite peculiar and logically somewhat inconsistent for several reasons:

a) The authors use only intracellular conductivities in monodomain simulations. This is equivalent to assuming that the conductivity of the interstitial current path is infinite. Therefore this choice tends to overestimate conduction velocities significantly. This is why most studies use harmonic mean conductivity values which adequately account for the conductivity of the

interstitial space. Such monodomain models are axially equivalent to bidomain models and thus predict virtually the same activation patterns as full-blown bidomain formulations. Based on the three reports on conductivities in the literature, harmonic mean conductivities along the fibers are 0.13, 0.123 and 0.089 S/m, and, in the transverse direction, 0.0176, 0.022 and 0.034 (values by Clerc, Rorberts 79, Roberts and Scher 82). Since conduction velocity is proportional to the square root of the harmonic mean conductivity the authors overestimate conduction velocity noticeably. In the longitudinal direction the overestimate by a factor of 1.6 over the fastest prediction based on measured conductivities, in the transverse direction the overestimate is lower (a factor of x 1.33).

- We thank the reviewer for catching this error in the listed equations. In fact in monodomain simulations, our software automatically calculates the bulk or harmonic mean conductivity values from the bidomain conductivities. We have now changed the equations and added a reference to rectify the mistake in the text. Thus, the values used in the simulations are actually 0.089 and 0.034 S/m in the longitudinal and transverse directions, respectively.

b) The authors picked the conductivities reported by Roberts and Scher which are the extremal values, where intracellular longitudinal conductivities are twice as large as those reported by Clerc, and in the transverse direction conductivities are three times larger. In combination with the use of intracellular conductivities instead of harmonic mean conductivities the speed of propagation is clearly overestimated. Consequently, the authors had to reduce the conductivities significantly to be get inducibility (by 30% to account for heart failure and, on top of this, by 70%).

- See explanation above.

These concerns do not question the validity of the method for estimating fiber orientations, nonetheless, a rationale for this particular choice of parameters should be given.

Another concern is the incomplete comparison with alternative methods which could results in equally good estimates of fiber orientations such as, for instance, rule based methods, a technique that has been used by the authors in previous studies themselves.

- We agree that alternatives such as rule-based methods offer estimates of fiber orientations. But these alternatives have certain limitations which the proposed methodology overcomes, as discussed in our IEEE TMI paper. We have now explicitly stated this in the Introduction section and cited our IEEE-TMI paper.

Data in the text of section "Representative Results", second par, do not seem to match up very well with the corresponding Fig. 11. Fig. 11B suggests that in some regions, mostly close to the base, the overall mean difference was 20 ms. In the text the authors claim that the overall mean difference was 5.7 ms. Is this averaged over all mean differences? Further, the authors say that the 5.7 ms correspond to 3.7% of the total activation time, suggesting that the total activation time was close to 157 ms for the normal heart. Activation plots suggest that activation was very slow indeed (color bars are up to 200 ms). In normal humans the normal QRS duration is around 60-100 ms which is significantly smaller. I would assume that in a canine model total activation time would be even smaller due to the smaller size of the heart. The same concern applies to the data reported for the failing canine models where total activation time is as large as 500 ms. Assuming that propagation is mainly transmural in the case of a sinus beat, such long activation times suggest extremely slow decremental conduction velocities. Experimental studies, for instance by Poelzing and Rosenbaum, AmJPhysiol 2004, measured transmural activation times in the failing canine heart and reported a total transmural activation time of around 40 ms, suggesting that there is a discrepancy with the simulated data.
As outlined above, the choice of conductivities would lead to fast conduction velocities, yet the shown activation sequences are too slow which is somewhat surprising.

- The overall mean difference in activation times that we refer to is indeed the average of all mean differences. This has now been explicitly mentioned in the manuscript. As explained above, the bulk conductivity values used in the monodomain equations were on the low side with respect to other published values which contributes to the overall slowed conduction in the tissue. In addition, as shown in Fig. 10, we simulated activation during sinus rhythm by stimulating 6 sites on the endocardium. Increasing the bulk conductivity values or adding more stimulation points from the endocardium would yield faster total activation times that would better match experimental data. But the results with respect to testing the effects of fiber estimation on simulation results will still be the same.

Minor Concerns:
In the last par of the Introduction, line 4 from bottom, an "and" is missing in "mathematical techniques AND experimental data"

- Corrected, thank you.

Protocol text, section 2.1.), last line: "... via radio frequency ablation of the left bundle branch block ...", remove block

- We have removed “block.” Thank you.

Figure 4D is not referenced in the text in section 1.3, nor is it referred to in the figure caption.

- We have corrected Figure 4. Thank you.

Although figures are not numbered in the manuscript, to me it seems as if figures 9 and 10 are swapped if the sequence in which figures appear in the manuscript is an indication of the figure number.

- There was an error in figure numbers. It is now corrected. Thank you.

The description of the lead vector is insufficient, perpendicular to the apico-basal axis can mean many different things. With this vague description one cannot interpret the ECG signals shown later in the manuscript.

- We have added more detail in the text and modified Fig. 10 to illustrate the location of the lead vector.

The meaning of \bar{X} and \bar{Y} in the equation used to compute the MAD metric are probably the mean of ECGs obtained with acquired and estimated fiber orientations, but this should be spelled out explicitly in the text.

- The meaning of \bar{X} and \bar{Y} have now been mentioned.

In Fig 11, the color bar indicates that the scale for errors in inclination angle was up to 180 degrees. In my view the largest possible error in inclination angle is 90 degree. In terms of fiber orientation, a 180 degree difference in fiber orientation means a zero error. This should be clarified. 20-25% of the inclination angles are off by more than 20 degrees, when considering that the maximum deviation is 90 degrees, this is a fairly large estimation error.

- We appreciate the reviewer's concern. We used inclination angles to define error, following the tradition of histology. The inclination angle by definition varies between -90 and +90 degrees, and consequently, the error, i.e, absolute difference between inclination angles, varies between 0 and 180 degrees. The Introduction section (last paragraph) and the Representative Results section (first paragraph) have been updated to specifically mention these. When comparing fiber orientations, it is common to compute the difference between inclination angles (e.g., Scollan et al. in the manuscript) without any adjustments for range, and we have adopted this commonly used approach to quantifying fiber orientation error. We agree with the reviewer that our definitions sometimes lead to overestimation of errors. But this is an inevitable consequence of defining the error in terms of the traditional characterization of fiber orientations, i.e, inclination angles. However, only 1.5% and 2.5% of voxels have errors larger than 90 degrees in normal and failing hearts, respectively. So the extent to which the overestimation affects the results is very low. Despite the overestimation, the error

values are small, and this shows that the proposed methodology works well. For the readers who are interested in the acute angle between fibers, which varies between 0 and 90 degrees as this reviewer points out, we have now provided the mean 3D acute angles in the manuscript (see 2.6 and first paragraph of the Representative Results section). Thank you.

In "Representative Results, par 2, last line on page, the authors refer to Fig. 5C, but I assume their intention was to refer to Fig. 12C.

- Thank you for this correction. The text now refers to the correct figure.

The CARP software used for simulating activation sequences is not listed in the table.

- CARP is now listed in the table. Thank you.

Reviewer #2:

Summary:

The aim of the study is to provide a method to infer cardiac fiber architecture from cardiac geometry and assess its performances when simulating cardiac electrophysiology.

- We thank the reviewer for his/her time and feedback.

Major Concerns:

1. Why do you present human heart data whereas you do not use it in your experiments?

- As we have already mentioned in the last paragraph of the Introduction section, we do not have access to DTMR images of multiple human hearts to perform our experiments. It is very challenging to obtain healthy human hearts for research, as they are needed for transplantation.

2. Experiments are done on canine hearts, how can you extend it to clinical applications on human hearts? There is a link missing...

- We appreciate the reviewer's concern. It has not been possible for us to obtain DTMR images of multiple human hearts to perform our validation experiments (see our response to the previous comment). However, we expect that the methodology will accurately estimate fiber orientations in human hearts as well because, just as in canine hearts, fiber orientations relative to geometry have been shown to be similar between different human hearts, as demonstrated by Lombaert *et al*. (reference [15] in revised manuscript). The final paragraph of the revised manuscript now states these.

3. To be discussed, what about using a statistical atlas instead of a single sample atlas? cf. [Peyrat, TMI 2007] and [Lombaert, TMI 2012]

- Thank you for raising this important question. We have now reported the standard deviation of errors across the 5 different estimates of the fiber orientations of heart 1. The accuracy of the estimation of fiber orientation of heart 1 does not vary significantly when different atlases are used, and accordingly, we expect that a statistical atlas is not required for the purposes of our study. The manuscript has been modified to mention these (Paragraph 1 of Representative Results, and paragraph 2 of Discussion).

4. The conclusion is that solely geometry matters for fiber orientation, I would not be so affirmative. It might be true but only for the type of failures that were used in the experiments. A lot of work exist to study the impact of infarcts and fiber organization in electrophysiology (reentry problems...). Maybe the fiber orientation does not matter as much as conductivity parameters that are similar in your experiments for both cases compared...

- We agree with the reviewer in that further testing of the proposed methodology is necessary. The last paragraph of the discussion section now explicitly mentions that further testing of the proposed methodology under other disease conditions, especially myocardial infarction, is important.

6. You only compare inclination angle which is not a fully 3D representation of fiber orientation. What about differences in other projection planes?

- The inclination angle measure was chosen following the tradition of histology. Since the angle between the fiber direction and epicardial tangent plane is generally small, the information loss in describing a fiber direction entirely using its inclination angle is insignificant. The manuscript now mentions these (see Introduction, last paragraph). For readers interested in angular errors in 3D, the manuscript now reports the mean 3D acute angle between estimated and acquired fiber directions, in paragraph 1 of Representative Results section. Thank you.

7. How do you reconstruct ventricular models? What is the resolution of meshes you use? Could the absence of differences due to the level of resolution chosen for these experiments? This is necessary in the description to ensure reproducibility

- As we had already mentioned with citations in the last paragraph of the Introduction section, the models were reconstructed using previously published methods. We agree that the resolution information is necessary for reproducibility, and this information has now been provided under 3.1. Error analysis of our numerical technique showed that solutions converged when the finite element mesh has average edge length < 600 microns. Meshes with larger average edge length led to overestimation of conduction velocity in the models.

5. Bibliography is lacking, most references come from their own lab. Especially concerning cardiac fiber architecture: [Sundar, ISBI 2006], [Rhomer, Inv. Rad. 2007], [Gilbert, EJCS 2007], [Peyrat, TMI 2007], [Lombaert, TMI 2012], and clinical applications [Sermesant, MedIA 2012]. And what about work on in vivo DT-MRI acquisition?

- Thank you for providing additional references. They have now been cited in the manuscript. Also, we have provided a citation to our IEEE Transactions on Medial Imaging paper, where a brief description of the previous work on in vivo DTMRI can be found (see second paragraph, Introduction section).

Minor Concerns:

1. Why LDDMM and not other techniques? Why is diffeomorphism necessary?

- We have now mentioned in the 3rd paragraph of Introduction why the diffeomorphic property is important. LDDMM also ensures that the geometric transformation defines a geodesic path in the space of diffeomorphisms, thereby providing a metric quantification of the difference between the atlas and patient. While geodicity is not

essential for fiber orientations estimation, from the standpoint of our long-term goals in patient-specific cardiac image analysis, it is a desirable property.

2. Why is PPD used to reorient tensors and not FS?
    - A detailed comparison of various reorientation strategies is not within the scope of our manuscript. We chose PPD because our results showed that it outperformed FS. Interested readers can find mode details in our IEEE Transactions on Medical Imaging paper, which is cited numerous times in the manuscript. Thank you.

Reviewer #3:

Summary:

This paper presents the application of mapping fibers from a normal heart to a failing heart and looking at the error in fiber orientation and differences in pseudo ECG simulation.

- We thank the reviewer for his/her time and feedback.

Major Concerns:

This is an interesting topic but I have major concerns regarding the contributions of this particular manuscript as well as the conclusions:

The method applied is the one already described in [3]. The exact same pipeline is used here, using data sets from the same origin. The obtained results draw the same conclusion that was already found by the people who acquired this data: as also already described in [6], there is no drastic changes in the fiber orientations of these failing hearts, therefore it is expected that mapping healthy fibers will provide similar orientations and simulations. On the simulation side, it is using an already published approach. The conclusion is that the pseudo ECGs are similar, which is logical given that the fibers are similar. There is a large amount of publications on the influence of cardiac tissue anisotropy on local activation time and ECG simulations. Finally the variability of the fibers in this publicly available DTI datasets has already been deeply studied and published. Additional references on these last two topics (analysis of this ex vivo DTI data and influence of anisotropy on simulations) are missing, while it is the core of the article.

- We appreciate the reviewer's concern that the methodology and results described in this JoVE article have already been published by IEEE Transactions on Medical Imaging (IEEE-TMI) journal. However, as per our agreement with the editorial office of JoVE, the purpose of the present manuscript is to disseminate previously accepted and published methodologies in the video format. Thus, even though the present manuscript does not contain novel research, it will publicize existing research in a novel and easily accessible manner. The purpose of this article is not a detailed study of how anisotropy affects simulations, but to demonstrate that the inter-subject variability of relative fiber orientations is low enough to facilitate accurate estimation of fiber orientations for patient-specific simulations.

  To address the reviewer's comment on additional references, the revised manuscript cites papers on analysis on ex vivo DTMRI data, including those of Helm et al, Peyrat et al, and Lombaert et al. We have also added two additional references (by Wei et al. and Leon et al.) on the influence of anisotropy on simulations.

Moreover, I disagree with the message of this article. In this precise case of an animal model of dilated cardiomyopathy artificially created by generating a LBBB, the fibers are close to healthy orientations. But it is not known if a genuine DCM will not remodel the fibers differently. Moreover the largest impact of cardiac fiber orientations on the electrophysiology in patients comes from local changes in orientation due to the pathology, as the disarray around an infarcted region or small channels in the border zone. Therefore the conclusion saying that we can use fiber orientations from a healthy heart in order to do patient-specific simulations is not holding in many cases.

- According to the publication that describes the acquisition of the data used in our manuscript, the experimental canine model that we use has been well described in the literature as one that reproduces many of the molecular, cellular, and structural features of human dilated cardiomyopathy (see Helm et al, reference [11]). We agree with the reviewer in that it is important to test the proposed methodology under myocardial infarction. This limitation of the present study has now been mentioned in the last paragraph of Discussion.

Minor Concerns:

I do not see why the MAD is a good metric for comparing ECGs. In its statistical definition, it will reduce the influence of outliers in the difference, while it is what we are looking for as the ECG are close to 0 for a large part of the cardiac cycle, therefore the difference will be small most of the cycle anyway. Moreover, it outputs 0 if there is a time shift but exactly the same ECG. The comparison should be more detailed.

- We appreciate the potential limitations of the MAD metric that the reviewer mentioned. But the MAD metric has been utilized in clinical studies, to compare ECGs of reentrant activity and paced propagation for localization of the organizing centers of reentrant circuits. A MAD score of less than 12% implies that the two underlying propagation patterns are clinically equivalent. The manuscript now includes these details with relevant reference (second paragraph in Discussion)